Time-dependent pleiotropic phenotypes are caused by progressive DNA polymerase α deficiency in zebrafish

Alex Y. Lin[1,2], Georgia K. Thomas[1,2], Khai Chung Ang[1,2], Damian B. van Rossum[1,2], Victor A. Canfield[1,2], and Keith C. Cheng[1,2]*

[1]The Jake Gittlen Laboratories for Cancer Research, Penn State College of Medicine, Hershey, PA, USA;

[2]Division of Experimental Pathology, Department of Pathology, Penn State College of Medicine, Hershey, PA, USA

*kcheng76@gmail.com (KCC)

Short title: Pol α deficiency mediates cell-specific atypia and cell death

Keywords: Pol α, *pola2*, nuclear atypia, cell death, zebrafish

Abstract

The mechanisms underlying variation in cell- and tissue-specific phenotypes caused by mutations are poorly understood. For example, why some cancers show cellular atypia more than others is unclear. As an illustration of phylogenetic variation in phenotype, mutations in a subunit of DNA polymerase α (Pol α), one of the primary eukaryotic replicative DNA polymerases, result in immediate cell cycle arrest in yeast and *Arabidopsis*; a null mutation in the same subunit results in lethality in 5 to 7 days in zebrafish, in association with striking tissue-specific, time-dependent pleiotropic cellular phenotypes. Here, we describe a zebrafish null mutant in the gene encoding the B subunit of Pol α, *huli hutu* (*hht)*, in which cell death with nuclear fragmentation is found in the central nervous system where the largest number of cells arise, while cells present in smaller numbers, such as the gastrointestinal epithelial cells, instead show cellular atypia that is associated with hepatic dysgenesis and pancreatic and air bladder agenesis. Wild-type maternal mRNA in genotypically mutant eggs becomes undetectable by 24 hours post-fertilization (hpf). Furthermore, the treatment of wild-type larvae with DNA synthesis inhibitors aphidicolin or hydroxyurea from 24 hpf phenocopies *hht*. Taken together, the data are consistent with a model in which reduced capacity for cell proliferation caused by either genetic or chemical mechanisms of DNA synthesis beginning at about 24 hpf results in cell death in tissues with large cell number, and abnormal nuclear morphology in tissues with fewer cells, including the gastrointestinal tract.

48 **Introduction**

49 Changes in nuclear morphology occur during normal cellular processes such as mitosis,
50 differentiation, and cell migration (Jevtić *et al*. 2014, Calero-Cuenca *et al*. 2018), but
51 histologically-defined cellular atypia, characterized by darker hematoxylin staining and large,
52 irregular nuclear shape, is common in both neoplasia and in settings that involve physical or
53 chemical damage to DNA, such as UV-irradiation and chemotherapy (Blum 1978, Stenbäck 1978,
54 Carr and LiVolsi 1989, Kim *et al*. 2016). Nuclear atypia is also used as a diagnostic signature in
55 many human cancers and pre-cancers (Rosai 2004, Billings and Goldblum 2010, Kumar *et al*.
56 2010, Lanzkowsky *et al*. 2016, Pizzorno *et al*. 2016). The presence and severity of nuclear atypia
57 generally correlates with higher tumor grade and poor prognosis (Rosai 2004, Kodota *et al*. 2014,
58 Manimaran *et al*. 2014, Yamaguchi *et al*. 2015, Poropatich *et al*. 2016, Zhou 2018). Despite the
59 clinical diagnostic relevance of nuclear atypia, its genetic and mechanistic origins are poorly
60 understood.

61

62 The small size of zebrafish larvae allowed us to generate histological arrays for pursuit of a
63 histology-based forward genetic screen to identify genes that can cause nuclear atypia (Mohideen
64 et al. 2003). Our laboratory identified a recessive larval-lethal mutant, *huli hutu* (*hht*), that develops
65 optical opacity of the brain, small eyes, an upward curvature of the body, and dies after 5 to 7 days
66 of development. Histology revealed that virtually all organs and tissues exhibited severe
67 cytological abnormalities (Mohideen *et al*. 2003). Highly proliferative tissues, particularly of the
68 retina and brain, and to a lesser extent, the gastrointestinal tract organs, were affected most
69 dramatically.

70

71 Positional cloning shown here revealed a frameshift mutation in *pola2* in *hht*, which encodes the
72 B subunit of the DNA polymerase α-primase complex (Pol α). Immediate growth arrest
73 phenotypes associated with *pola2* mutation in two other organisms, *Saccharomyces cerevisiae*,
74 (Foiani *et al* 1994) and *Arabidopsis thaliana* (Yang *et al.* 2009) begged the question of the reason
75 underlying the longer survival of zebrafish *pola2* mutants. In *Caenorhabditis elegans*, mutation
76 of the *pola2* paralog *div-1* substantially increased the duration of interphase and produced embryos
77 that failed to hatch or to generate intestinal or pharyngeal cells (Encalada *et al.* 2000). We detected
78 wild-type maternal *pola2* mRNA in homozygous mutant embryos, providing an explanation for
79 the extended lifespan of *pola2* mutant zebrafish. Consistent with the disappearance of detectable
80 *pola2* mRNA at 24 hpf, two independent chemical means of inhibiting DNA synthesis beginning
81 at 24 hpf phenocopied cell-specific *hht* phenotypes. Here, we show correlations between
82 replicative demand and DNA damage that appear to explain the disparity in mutant phenotype
83 between cell types.

84 **Results**

85 ***A zebrafish mutant with abnormal nuclear morphology***

86 The gross phenotype of *hht* mutants is evident at 3 days post-fertilization (dpf) under a dissecting
87 microscope and includes reduced head and eye size, a curved body, and a pronounced yolk
88 (Mohideen et al. 2003, **Fig. 1A**). Further characterization by 3-dimensional x-ray histotomography
89 using micro-CT confirmed that these mutants lack the pneumatic duct and swim bladder (Ding *et*
90 *al*. 2019). This gross phenotype persists until death, which occurs between 5 and 7 dpf (**Fig. 1B**).
91 A detailed examination by histology at 5 dpf showed that while all organs and tissues were
92 distinguishable, virtually all exhibited severe cytological changes (**Fig. 1C**). Highly proliferative
93 tissues, including retina, brain, and gastrointestinal tract organs, were affected most dramatically.
94 Enterocytes in the *hht* intestinal lumen were irregular in polarity, size and shape, cellular and
95 nuclear boundaries were difficult to define, and cell nuclei were often hyperchromatic and
96 contained prominent nucleoli. Other endodermally-derived organs such as pancreas and liver also
97 exhibited severe cytologic atypia, often presenting with enlarged nuclei and high variability in
98 cellular and nuclear size and shape. Dysmorphologies were also detected in cartilage, where the
99 normal aligned arrangement of cartilage cells in neat rows (in wild-type siblings) is replaced by
100 cells with variable shapes, sizes, and polarity, and irregular arrangements. The eyes of *hht* mutants
101 have misshapen lenses and retinas with a substantial reduction in cell number, a loss of
102 stratification of retinal layers, and nuclear fragmentation.

103

104 ***Pola2 mutation is responsible for the hht phenotype***

105 *Positional cloning indicates the causative mutation is in one of five candidate genes*

106 Microsatellite-based positional cloning and gene knockdown by morpholino oligonucleotides
107 revealed that the causative gene in *hht* mutants was *pola2*. The identification of zero recombinants
108 in 1948 meioses with markers *z10868* and *z15236* revealed that the gene responsible for the *hht*
109 phenotype was less than 0.05 centimorgans (cM) away, which corresponds to about 35.5 kb in
110 zebrafish (Shimoda *et al*. 1999). These two markers were flanked on either side by microsatellite
111 markers *z26580* and *z13225*, each of which had one recombinant in 1948 meioses, indicating that
112 the causative mutation resides between these markers (**Fig. 2A**). Five candidate genes, *cenph*,
113 *dimt1l*, *mier3b*, *mrps36*, and *pola2*, are annotated in this region.

114

115 *Morpholino antisense knockdown of pola2 results in hht phenotype*

116 To identify the gene responsible for the *hht* phenotype, one translational blocking and two splice-
117 junction blocking morpholino oligonucleotides (MOs) were designed per candidate gene and
118 injected into wild-type zebrafish embryos at the one-cell stage to inhibit translation or RNA
119 splicing, respectively. Only *pola2* and *dimt1l* morphants exhibited a combination of reduced head
120 and eye size, a pronounced yolk, and a dorsal curvature that were grossly similar to *hht*
121 (**Supplemental S1**). Histological examination of cellular phenotype at 3 dpf revealed striking
122 similarities between *pola2* morphants and *hht*, both demonstrating reduced retinal volume and cell
123 number, loss of retinal layers, fragmented cell nuclei, and a thickened uneven corneal epithelium
124 (**Fig. 2B**). The eyes of *dimt1l* morphants, while distinctly abnormal compared with wild-type
125 zebrafish, retained the overall size, ovoid shape, some retinal layering, and cell types of wild-type
126 eyes, and lacked the profound deficiencies found in *hht* eyes. Taken together, mapping data and

127 the near identity in phenotypes of *hht* and *pola2* morphants indicate that the affected gene in *hht*
128 is *pola2.*
129
130 Sequencing of gDNA and cDNA of wild-type and mutant *pola2* revealed a 2-nucleotide AC
131 insertion at the double AC repeat at the 68th nucleotide from the translation start site (**Fig. 2C**).
132 The frameshift mutation results in a premature stop codon at the 38th amino acid position (**Fig.**
133 **2D**), suggesting that the final protein product is truncated and non-functional. The AC insertion,
134 located at the 2nd exon of the 19-exon zebrafish *pola2* gene, is therefore most likely the causative
135 mutation. To verify this insertion, genomic DNA from 20 each of *hht* larvae and wild-type larvae
136 from wild-type siblings of their parents was pooled to sequence PCR amplicons of the 2nd exon of
137 *pola2;* the 2-nucleotide insertion was present in the *hht* pool, but not the wild-type pool.
138
139 <u>*Partial rescue of the huli hutu mutant phenotype with wild-type pola2 mRNA*</u>
140 One prediction of *pola2* being the affected gene in *hht*, is that injection of wild-type mRNA would
141 rescue at least some of the several phenotypes of *hht* fish. Wild-type *pola2* mRNA was transcribed
142 from a cDNA clone from the wild-type Connors background strain and injected into embryos from
143 a $\frac{hht}{+}$ x $\frac{hh}{+}$ cross at the 1-cell stage with the expectation of a 1:2:1 ratio of $\frac{+}{+}$, $\frac{hht}{+}$, and $\frac{hht}{hh}$
144 genotypes (**Supplemental S2**). At 3 dpf, 90% of injected $\frac{hht}{hht}$ larvae, identified by genotyping,
145 were partially rescued, exhibiting an intermediate gross phenotype – a straight body and yolk
146 resembling that of a wild-type, but with eyes and brain that are smaller than wild-type but larger
147 than *hht* (**Fig. 3, Table 1**). This intermediate phenotype has not been seen in hundreds of crosses
148 between *hht* heterozygotes. All larvae with an intermediate phenotype were genotypically
149 homozygous mutant ($\frac{hh}{hht}$). Retinal cell layering of the rescued fish was reminiscent of those seen

150 in homozygous wild-type larvae. The *hht* intestinal epithelial phenotype, in which cell nuclei show
151 loss of polarity and prominent nucleoli, was absent in mRNA-rescued *hht* larvae. Fragmented
152 nuclei in the brain and eyes of *hht* larvae were also absent in both wild-type and rescued fish. The
153 incomplete rescue phenotype can be explained by an expected degradation and/or dilution of the
154 injected wild-type *pola2* mRNA over time, leading to a slower rate of cell division than in wild-
155 type fish.
156
157 Another prediction of *pola2* mutation being responsible for the *hht* phenotype is that knockout of
158 *pola2* on both chromosomes by genome editing would show a *hht* phenotype. Wild-type larvae
159 were rendered mutant for *pola2* using the CRISPR/Cas9 genome editing system. Homozygous
160 knockout fish harboring a 16-nucleotide insertion between nucleotides 927-928 (**Supplemental**
161 **S3A**) exhibited a gross phenotype that was strikingly similar to *hht* (**Supplemental S3B**). The
162 frameshift in this CRISPR insertion allele disrupts the protein sequence after amino acid 308.
163 Under the assumption that human and zebrafish POLA2 proteins share similar structures, these
164 *pola2* knockout zebrafish would produce a mutant protein without a functional phosphodiesterase
165 (PDE) domain, which has been reported to be important for binding between human POLA2 and
166 the catalytic A subunit of Pol α, predicting a null phenotype (Klinge *et al*. 2009, Suwa *et al*. 2015).
167 The gross phenotypes of *hht* and *pola2* knockout larvae were indistinguishable, further confirming that the
168 affected gene in *hht* is *pola2*.
169
170 We have established that *hht* is mutant in the *pola2* gene by positional cloning, morpholino
171 knockdown to generate a similar histological phenotype, CRISPR knockout, and partial rescue
172 with *pola2* mRNA. Human POLA2 protein, the B subunit of DNA polymerase alpha, is known to

173 mediate binding of the A catalytic subunit and the chromosome (Suwa *et al.* 2015). As predicted
174 by this model, insertional mutant of the A subunit, encoded by *pola1*, resulted in gross and
175 histological brain and eye phenotypes indistinguishable from *hht* mutants (**Supplemental S4**).
176

177 ***pola2-deficient zebrafish mutants exhibit reduced DNA synthesis***

178 Since *pola2* plays a critical role in DNA replication, we investigated how DNA synthesis was
179 affected in the *hht* mutants. Wild-type and *hht* larvae between 2 to 5 dpf were assessed for DNA
180 replication by incorporation of 5-ethynyl-2′-deoxyuridine (EdU), a synthetic thymidine analog.
181 After 30 min of EdU incubation, wild-type larvae exhibited strongly positive EdU staining at all
182 ages examined. In contrast, *hht* larvae were EdU-negative from 2 to 5 dpf, indicating a reduction
183 of DNA synthesis below the limits of detection (**Fig. 4**).
184

185 The observed global reduction of DNA synthesis in *hht* mutants suggests a model in which
186 inhibition of DNA synthesis by any mechanism can potentially reproduce the *hht* phenotype,
187 which includes largely normal development up to 24 hpf followed by progressive dysmorphology
188 and cell death. Based on this timing, we hypothesized that chemical inhibition of DNA synthesis
189 by multiple mechanisms may be able to phenocopy *hht*, if started at about 24 hpf. To test this idea,
190 wild-type larvae were exposed to hydroxyurea, an inhibitor of deoxyribonucleotide production, or
191 aphidicolin, an inhibitor of replicative DNA polymerases α, δ, and ε (Zhang *et al*. 2008), beginning
192 at different times. Wild-type embryos were treated with empirically determined concentrations of
193 50 μM aphidicolin or 150 mM hydroxyurea to induce the *hht* phenotype. Starting inhibition at 2
194 hpf resulted in death by 24 hpf (**Fig. 5A**). Inhibiting DNA synthesis beginning at 24 hpf (but not

195 before) phenocopied *hht* by 72 hpf (**Fig. 5B; Supplemental S5, S6**). Cellular phenotypes in the
196 eyes, brain, and intestine were confirmed by histology (**Supplemental S7**).
197
198 Since inhibition of DNA synthesis predicts cell cycle arrest in S phase, higher proportions of cells
199 are expected to be in S phase. We measured the proportion of cells in S phase by flow cytometric
200 measurements of DNA per cell in propidium iodide-labeled cells dissociated from wild-type and
201 *hht* larvae (**Fig. 6**). At 3 dpf, the proportion of cells in S phase was approximately 3-fold higher in
202 *hht* (45.9 ± 5.8 %) than in wild-type (15.5 ± 3.2 %; $p < 0.05$, t-test). S phase accumulation in *hht*
203 cells persisted to 5 dpf ($p < 0.05$, t-test). In this analysis, all cell types were examined and the
204 proportion of cells in each phase of the cell cycle represented an average across heterogeneous cell
205 populations.
206
207 ***Tissue specificity of cell death and DNA damage phenotypes in* hht *zebrafish***
208 Nuclear fragmentation as seen in the eyes of *hht* larvae indicates cell death. To assess the extent
209 and timing of cell death, live wild-type and *hht* larvae at 24, 36, 48, 72, 96, and 120 hpf were
210 incubated with acridine orange (AO), a fluorescent vital dye that labels dying cells. There was no
211 significant difference between the number of AO-positive foci in wild-type and *hht* larvae at 24
212 hpf but AO-positive foci in *hht* larvae increased dramatically between 24-36 hpf (**Fig. 7A**). After
213 peaking at 36 hpf, the number of detectable foci in *hht* continued to decline until 120 hpf. In
214 contrast, the number of AO-positive foci in wild-type larvae remained consistently low and was
215 significantly less than in *hht* larvae - at the 36 hpf peak, the number of AO-positive foci in *hht* was
216 approximately 4-fold higher than that in wild-type. AO-positive cells in *hht* larvae accumulated

217 predominantly in the most numerous cell types – those in the brain, eyes, and spinal cord (**Fig. 7B-**
218 **C**).
219
220 To assess the induction of double strand DNA breaks, wild-type and *hht* larvae at 24, 36, 48, 72,
221 96, and 120 hpf were probed with an antibody specific for γ-H2AX, the phosphorylated form of
222 H2AX, a member of the H2A histone family. H2AX becomes phosphorylated on serine139 in
223 response to double-stranded DNA breaks (DSB, Kuo and Yang 2008). At all ages examined, less
224 than 30 positive foci were detected per wild-type larva. In contrast, the number of positive γ-H2AX
225 foci in *hht* was indistinguishable from wild-type at 24 hpf, but increased significantly, from 8- to
226 13-fold, between 36-120 hpf. (**Fig. 8A**). γ-H2AX staining predominated in the brain, eyes, and
227 spinal cord of *hht,* following the pattern of cell death as assessed by AO (**Fig. 8B-C**).
228
229 ***Wild-type maternal* pola2 *mRNA sustains survival of* pola2*-deficient mutants***
230 To explain the extended survival of *pola2* null mutants of zebrafish compared with the *pola2*-
231 deficient phenotypes of other model organisms, we hypothesized the presence of wild-type
232 maternal *pola2* mRNA contributed from the wild-type chromosome of the heterozygous mother's
233 primary oocytes. Wild-type Pola2 protein originating from translation of wild-type maternal *pola2*
234 mRNA would then support normal DNA replication during early embryogenesis and could be
235 expected to be progressively diluted as cells divide in the absence of the wild-type gene in *hht*
236 mutants. This scenario explains the relatively normal appearance of *hht* fish at 24 hpf, followed
237 by the increasing disruption of development and eventual death at days 5-7 that characterize *hht*
238 fish. The similarity in *hht* and chemically-inhibited fish phenotypes only after 24 hpf suggested
239 are consistent with active DNA replication before 24 hpf in *hht* homozygotes.

240

241 To determine whether maternal wild-type *pola2* mRNA facilitates the survival of *hht* larvae,
242 cDNA from 3 homozygous wild-type and 3 *hht* embryos at 2.5, 6, 24, 48, and 72 hpf were analyzed
243 by quantitative allele-specific PCR to detect the presence of wild-type maternal *pola2* mRNA (**Fig.**
244 **9**). At 2.5 hpf, wild-type *pola2* transcripts were detected at similar levels in wild-type and *hht*
245 embryos ($n = 3$; $p > 0.5$, t-test). By 6 hpf, the quantity of wild-type *pola2* transcripts in *hht* embryos
246 was significantly reduced compared to wild-type embryos ($n = 3$; $p < 0.05$, t-test). Wild-type *pola2*
247 mRNA was not detected in *hht* larvae at or beyond 24 hpf. Taken together, our results are
248 consistent with a model in which the presence of wild-type *pola2* mRNA and protein is responsible
249 for the sustained survival of the *hht* mutants, and that the degree of depletion of *pola2* mRNA and
250 protein would be dependent upon the number of cell divisions in a given lineage.

251

252 **Discussion**

253 Nuclear atypia, despite its clinical importance in the diagnosis and prognosis of human cancers,
254 has not been clearly linked to the genetic origins of cancer. Since the amount of hematoxylin stain
255 in histology is roughly proportional to DNA content, aneuploidy is associated with darker staining
256 nuclei. Nuclei showing increased hematoxylin staining in nuclei, referred to as hyperchromatic
257 nuclei, are a component of nuclear atypia, and are often associated with increased prominence of
258 nucleoli and irregular nuclear shapes. Cells of the brain and eyes have dense nuclear morphology,
259 making it impossible to assess prominence of nucleoli as a component of nuclear atypia. In
260 contrast, the nuclei of gut cells are far larger. Since larger euploid cells contain the same amount
261 of DNA per cell as cells with small nuclei, their nuclei are normally largely pale, with darker-
262 staining nuclear regions. The atypical nuclei of *hht* gut epithelium are consistent with hyperploidy,

263 which can be caused by arrest of DNA replication in S phase. Cells trapped in S phase in *hht*
264 mutant cells that are still alive would, by definition, contain more than 2n DNA content, and
265 therefore be more darkly stained.
266
267 The tissue-dependent cellular phenotypes caused by *pola2* deficiency in *hht* mutants are consistent
268 with differences in cell proliferation in different cell types. Since homozygous *hht* mutants cannot
269 generate wild-type *pola2* mRNA, the quantity of wild-type *pola2* mRNA, and presumably wild-
270 type Pola2 protein, is diluted after each round of cell division (**Fig. 10**). As shown in our RT-PCR
271 experiment, wild-type *pola2* mRNA is undetectable in *hht* fish by 24 hpf, leaving only the wild-
272 type Pola2 protein produced before the maternal-to-zygotic transition, to support growth thereafter.
273 Assuming the quantity of wild-type Pola2 protein in the progenitor cells for every tissue was the
274 same, and is diluted with each cell division, tissues with a larger number of cells must have
275 undergone more cell divisions and would thus contain less wild-type protein per cell. The
276 difference in cell number in different tissues may result from differences in proliferation between
277 organs.
278
279 The *pola2* gene encodes the B subunit of Pol α and does not itself exhibit any known enzymatic
280 activity. Molecular studies in mouse revealed that the B subunit is tightly associated with the zinc
281 finger motifs in the carboxy-terminal domain of the catalytic subunit A (Mizuno *et al.* 1999). It
282 functions as a "molecular tether" that recruits the catalytic polymerase subunit to the origin
283 recognition complex (ORC) for the initiation of DNA replication (Collins *et al* 1993; Uchiyama
284 and Wang 2004). Mutagenesis of the *POL12* gene, encoding the B subunit of Pol α in yeast,
285 showed that mutations in the conserved C-terminus of the protein caused either lethality or

286 temperature sensitivity while mutations in the non-conserved regions in the N-terminus had no
287 effect (Foiani *et al*. 1995). The B subunit has been shown to be phosphorylated and
288 dephosphorylated in a cell cycle-dependent manner and this phosphorylation is dependent on its
289 association with the catalytic subunit (Foiani *et al* 1995; Ferrari *et al* 1996). The ability of Pol α to
290 initiate DNA replication is maximized when the B subunit is phosphorylated while the N-terminus
291 of the catalytic subunit A remains unphosphorylated (Schub *et al*. 2001). Other studies have shown
292 that the B subunit pays a role in telomere maintenance in yeast (Grossi *et al*. 2004) and
293 reprogramming the regenerative potential of the tail fin of adult zebrafish (Want *et al.* 2019).
294
295 In non-vertebrate models, inactivating *pola2* mutations can result in immediate growth arrest (*S.*
296 *cerevisiae*: Collins *et al*. 1993, Foiani *et al.* 1994, Foiani *et al.* 1997; *Arabidopsis*: Yang *et al.*
297 2009). Despite the high likelihood that the *hht* zebrafish are null mutants, they exhibit an extended
298 lifespan of 5-7 dpf. As predicted by our replicative deficiency model, chemical inhibition of DNA
299 replication in wild-type embryos starting at 1 dpf phenocopied *hht* at 3 dpf. Treatment during early
300 embryogenesis caused death in wild-type larvae by 1 dpf, suggesting that normal DNA replication
301 is indeed required during early embryogenesis for the survival of *hht* mutants, just as it is required
302 in yeast and *Arabidopsis*. The detection of wild-type *pola2* mRNA in homozygous mutant embryos
303 supports our hypothesis that DNA replication during embryonic stages of the mutants requires
304 wild-type *pola2* mRNA. Since the homozygous mutant embryos have no genomic source for wild-
305 type *pola2* transcripts, wild-type mRNA must have come from the heterozygous mother (fathers
306 are also heterozygous but do not contribute mRNA to the oocyte). The maternal-to-zygotic
307 transition (MZT) designates the time at which the zygotic genome is activated, and maternal
308 transcripts become destabilized and rapidly degraded. In zebrafish, the transcription of the zygotic

309 genome begins around 3 hpf, and most of the maternal transcripts are degraded by 6 hpf (Kane
310 and Kimmel 1993, Schier 2007, Tadros and Lipshitz 2009). The time interval between MZT and
311 onset of the *hht* mutant phenotype suggests that persistence of the wild-type protein is responsible
312 for the survival of the mutant. That the pattern of subsequent somatic depletion of wild-type Pola2
313 protein in *hht* follows the pattern of DNA damage is consistent with our model for explaining the
314 cell-specific pattern of *hht*'s pleiotropic mutant phenotype.
315
316 The extended lifespan of our *pola2* mutant, *hht,* and its development of time- and tissue-specific
317 cellular abnormalities created an opportunity to explore the potential role of the progressive loss
318 of DNA replication in the causation of a diagnostically important tissue-specific phenotype
319 associated with cancer, nuclear atypia. We showed that the progressive pattern of phenotypic
320 change in *hht* can be explained by the initial presence of wild-type mRNA, followed by its
321 progressive loss in genotypically homozygous mutant zygotes. In the course of our work,
322 transcriptomic studies of wild-type, unfertilized zebrafish eggs showed that over 10,000 maternal
323 transcripts are present that include essential genes such as *pola2* (Rauwerda *et al*. 2016). The
324 present studies suggest that zebrafish mutants for maternally expressed essential genes may
325 provide an opportunity to assess, without bias, both the tissue-specific and potentially pleiotropic
326 effects of the progressive loss of gene function in the context of the whole animal. It is worth
327 noting that the tissue-specific phenotypes of *hht* were discovered here using histology, but that a
328 3-dimensional, pan-cellular, cell-resolution imaging method such as x-ray histotomography, will
329 be better-suited for the quantitative study of volumetric phenotypes such as cell and tissue volume
330 and shape across cell types and tissues (Ding *et al.* 2019). The incorporation of such approaches

331 in the systematic study of pleiotropy may help us to understand patterns of cell and tissue-specific

332 phenotypes that emerge in the course of disease.

333 **Materials and Methods**

334 **Fish lines, mating, and embryo collection**. Generation of ENU-mutagenized mutant *hht* was
335 previously described (Mohideen *et al*. 2003). The background strain was a wild-type fish line
336 acquired from the Connors fish farm, which differs from the Tu and AB laboratory strains that are
337 in common use. The *hht* line is maintained as heterozygotes due to the larval-lethal nature of the
338 mutation. Mating was carried out by placing male and female heterozygotes in Aquatic habitat
339 tanks with dividers the afternoon prior to egg collection. Collected eggs were disinfected in 10%
340 Ovadine (Syndel) for 1 min at room temperature then washed 3 times in charcoal-filtered water.
341 Larvae were incubated at 28.5° C to maintain consistent speed of development.

342 **Histology.** Procedure for zebrafish histology has been previously described (Copper *et al*. 2018)
343 Larvae were dechorionated prior to submersion in 10% Neutral Buffered Formalin (Fisher) at 4° C.
344 Samples were fixed overnight at room temperature with gentle agitation and subsequently
345 embedded in agarose. For long-term storage, fixative was replaced with 70% ethanol. Agarose-
346 embedded larvae are subsequently embedded in paraffin, sectioned, and mounted in glass slides.

347 **Sequencing.** mRNA was extracted from 72 hpf wildtype and *hht* larvae using the RNeasy Mini
348 Kit (Qiagen) and reverse transcribed to cDNA. PCR was performed on cDNA with 3 sets of
349 primers:

350 -23~596:

351 Forward (POLA2F1: TTGAACATCAGAGGACAATA)

352 Reverse (POLA2R1: TCTCCTCCGTCCAGCATCTC)

353 503~1274:

354 Forward (POLA2F2: AGAGGTGGTTTCCACATTTG)

355 Reverse (POLA2R2: ACAATACCAACTTGCATGC)

356 1180~1823:

357 Forward (POLA2F3: ACCAGGTGACAGAAACATTT)

358 Reverse (POLA2R3: TAAAGTTCAAACATTGTATG).

359 PCR was performed on gDNA with 1 set of primer for exon 2 of *pola2*:

360 Forward (POLA2F1: TTGAACATCAGAGGACAATA) anneals to the 5' end of the 2nd exon of

361 *pola2*.

362 Reverse (POLA2gR: TGACTCCAAACAATGTTGTACTTTGATAGTCATTTG) anneals to the

363 2nd intron of *pola2*.

364 PCR products were purified with the QIAquick PCR purification kit (Qiagen) and submitted to

365 Genewiz for sequencing.

366 **Genotyping.** Allele-specific primers were designed based on the SNAP primer method described

367 by Drenkard *et al*. Forward primers span the AC repeats. Wild-type specific primers detect alleles

368 with only two repeats and mutant specific primers detect alleles with three repeats.

369 Wild-type forward primer (POLA2wtF: CACTTTCAACATAGCCTTCAACAATGACAGC);

370 Mutant forward primer (POLA2mtF: GACACTTTCAACATAGCCTTCAACAATGAGACA);

371 gDNA reverse primer

372 (gPOLA2ASR: TGACTCCAAACAATGTTGTACTTTGATAGTCATTTG).

373 cDNA Reverse primer: (cPOLA2ASR: GCTCCAACATTTTGTCGATGGTGCC)

374 **RNA rescue**. Wild-type and mutant *pola2* mRNA was extracted from homozygous wild-type or

375 homozygous mutant embryos, respectively, from a $\frac{hht}{+}$ x $\frac{hht}{+}$ cross with the RNeasy Mini Kit

376 (Qiagen) and reverse transcribed into cDNAs using the M-MLV Reverse Transcriptase kit

377 (ThermoFisher). cDNA from wild-type embryos were subjected to allele-specific PCR to eliminate

378 heterozygotes. cDNAs were amplified by PCR with the following primers:

379 Forward primer (POLA2-BglIIF): AGATCTTTGAACATCAGAGGACAATA

380 Reverse Primer (POLA20MluIR): ACGCGTTAAAGTTCAAACATTGTATG

381 and cloned into PCR®II-TOPO® vectors for sequencing. After sequences are verified, the inserts

382 are subcloned into PT3TS(4) vectors. Plasmid DNA was extracted from competent cells with the

383 QIAprep Spin Miniprep Kit (Qiagen) and linearized with Xmal. mRNA was generated from the

384 linearized plasmids with the T3 RNA polymerase (NEB). 200 pg of wild-type or mutant *pola2*

385 mRNA were injected into embryos from a $\frac{hht}{+}$ x $\frac{hht}{+}$ cross at the 1-cell stage. All injected embryos

386 in the first round of rescue experiments were genotyped to ensure that no phenotypic wild-type

387 larvae were genotypically *hht*.

388 **CRISPR/Cas9 knockout.** Gene-specific primer was designed for *pola2* and annealed to a universal

389 primer containing the sgRNA scaffold as described in protocol provided by Dr. Wenbiao Chen's

390 lab at Vanderbilt University. 1 µL of 10 µM gene-specific primer was mixed with 1 µL of 10 µM

391 sgRNA scaffold primer, 2.5 µL 2X NEB buffer 2 with BSA and annealed at 98° C for 1 min then

392 cooled to 37° C with a ramp speed of 0.1° C/sec. 0.5 µL of 500 µM dNTP and 0.5 µL of T4 DNA

393 polymerase were added to the mixture and incubated for 20 min. T4 DNA polymerase was then

394 inactivated by incubation at 75° C for 20 min. sgRNA was synthesized using the MaxiScrip T7 kit

395 (ThermoFisher Scientific). 1 µL of Turbo Dnase I was added and incubated at 37° C for 15 min to

396 remove residual DNA primers. sgRNA was purified using the mirVANA kit (ThermoFisher

397 Scientific). 600 ng/µL Cas9 protein was mixed with either 100 ng/µL *pola2* sgRNA and injected

398 into wild-type zebrafish embryo at 1-cell stage.

399 pola2KO: ATTAATACGACTCACTATAGGGGTCCGCGCTGGATGGGGAAgttttagagctagaaatagc;

400 sgRNA scaffold: ttttgcaccgactcggtgccactttttcaagtTgataaCggactagccttattttaacttgctatttctagctctaaaac

401 **Cell cycle analysis.** 20 wildtype and *hht* larvae were collected at 3 and 5 dpf and dissociated into
402 single cells as previously described. Cells were resuspended in 2 mL 70% EtOH at room
403 temperature for 10 min to fix then stored at 4° C before use. Cells were centrifuged at 500 x g for
404 5 min to remove supernatant. 1 mL propidium iodide solution from DNA QC Particles Kit (BD)
405 was added to each cell mixture. Cells were sorted with FACSCalibur (BD) and cell cycle was
406 analyzed using ModFit LT V3.3.11.
407 **EdU staining.** For labeling of proliferating cells, 2, 3, 4, and 5 dpf wildtype and *hht* larvae were
408 incubated for 30 min at 28.5° C in 400 μM EdU solution (Life Technologies). Larvae were
409 incubated in charcoal-filtered water for 30 min at 28.5° C, then fixed immediately in cold 10%
410 neutral buffered formalin. Detection of EdU incorporation was performed according to
411 manufacturer's instructions. Samples were visualized with Axio Zoom.V16 fluorescence stereo
412 microscope (Zeiss).
413 **Chemical inhibition.** Wild-type embryos were submerged in charcoal-filtered water, hydroxyurea
414 (Sigma-Aldrich), or aphidicolin (Sigma-Aldrich) at 0, 2, 6 hpf or 24 hpf. For the 24 hpf treatment,
415 fresh solutions were administered at 48 hpf. Hydroxyurea was dissolved in deionized water to
416 prepare a 500 mM stock and aphidicolin was dissolved in DMSO to prepare a 10mM stock. Stock
417 solutions were diluted to appropriate concentrations for each experimental condition so that equal
418 volume was added.
419 **Acridine orange staining.** 24, 36, 48, 72, 96, and 120 hpf wildtype and *hht* larvae were incubated
420 in 2 μg/mL acridine orange for 30 min at 28.5° C, then washed for 5 min in charcoal-filtered water
421 for 5 min at 28.5° C. Larvae were visualized with Axio Zoom.V16 fluorescence stereo microscope
422 (Zeiss).

423 **γ-H2AX staining**. 24, 36, 48, 72, 96, and 120 hpf wildtype and *hht* larvae were fixed in cold 10%
424 neutral buffered formalin. Samples were permeablized in acetone at -20 °C for 7 min then washed
425 with distilled water for 5 min followed by two washes in PBS for 10 min. Samples were then
426 blocked in 5% goat serum for 1 hr at room temperature and incubated in 1:100 γ-H2AX primary
427 antibody (Genetex) overnight at 4 °C. After 3 washes in PBST for 15 min, samples were incubated
428 in 1:1000 Alexa Fluor 488 goat anti-rabbit secondary antibody (Life Technologies) for 3 hrs at
429 room temperature. After 3 washes in PBST for 15 min, samples were visualized with Axio
430 Zoom.V16 fluorescence stereo microscope (Zeiss).
431 **Wildtype *pola2* transcript detection.** DNA and RNA were extracted from 2.5, 6, 24, 48, and 72
432 hpf embryos with AllPrep DNA/RNA Mini Kit (Qiagen). Embryos were genotyped with allele-
433 specific PCR. RNA of genotyped homozygous wild-type and *hht* embryos were reverse transcribed
434 with oligo-dT. Quantitative PCR was performed on cDNA with allele-specific primers for wild-
435 type *pola2* and *actinb1*:
436 Forward (Actinb1F: CATCCGTAAGGACCTGTATGCCAAC)
437 Reverse (Actinb1R: AGGTTGGTCGTTCGTTTGAATCTC)
438 as loading control.
439 PCR products from three homozygous wild-type and mutant embryos were subjected to
440 electrophoresis. Relative quantity was calculated by densitometry as a ratio of *pola2*
441 product:*actinb1* product.

442 **Reference**

443

1. Aanes, H., Winata, C. L., Lin, C. H., Chen, J. P., Srinivasan, K. G., Lee, S. G. P., Lim, A. Y. M., Hajan, H. S., Collas, P., Bourque, G., Gong, Z., Korzh, V., Aleström, P., and S. Mathavan, 2011. Zebrafish mRNA sequencing deciphers novelties in transcriptome dynamics during maternal to zygotic transition. *Genome Res*. Aug; 21(8): 1328–1338.
2. Baranovskiy, A. G., Lada, A. G., Siebler, H. M., Zhang, Y., and Y. I. Pavlov, 2012. DNA polymerase δ and ζ switch by sharing accessory subunits of DNA polymerase δ. *J Biol Chem*. 287(21):17281-7.
3. Blum, H. F., 1978. Ultraviolet radiation and skin cancer in mice and men: accumulation of effect and uncertainty of prediction. *Natl Cancer Inst Monogr.* Dec; 50:11-2
4. Calero-Cuenca, F. J., Janota, C. S., and E. R. Gomes, 2018. Dealing with the nucleus during cell migration. *Curr Opin Cell Biol*. **50**: 35-41.
5. Carr, R. F. and V. A. Livolsi, 1989. Morphologic changes in the thyroid after irradiation for Hodgkin's and non-Hodgkin's lymphoma. *Cancer*. Aug 15; 64(4): 825-9
6. Collins, K. L., A. A. Russo, B. Y. Tseng, and T. J. Kelly, 1993. The role of the 70 kDa subunit of DNA polymerase alpha in DNA replication. *EMBO J*. 12: 4555-4566
7. Cooper, G. M, 2000. *The Cell: A Molecular Approach. 2nd Edition*. Sinauer Associates; Sunderland (MA). ISBN-10: 0-87893-106-6.
8. Date, H., Onodera, O., Tanaka, H., Iwabuchi, K., Uekawa, K., Igarashi, S., Koike, R., Hiroi, T., Yuaasa, T., Awaya, Y., Sakai, T., Takahashi, T., Nagatomo, H., Sekijima, Y., Kawachi, I., Takiyama, Y., Nishizawa, M., Fukuhara, N., Saito, K., Sugano, S., and S. Tsuji, 2001. Early-onset ataxia with ocular motor apraxia and hypoalbuminemia is caused by mutations in a new HIT superfamily gene. *Nat Genet*. 29 (2): 184-188

465 9. Ding, Y., Vanselow, D. J., Yakovlev, M. A., Katz, S. R., Lin, A. Y., Clark, D. P., Vargas,
466 P., Xin, X., Copper, J. E., Canfiend. V. A., Ang, K. C., Wang, Y., Xiao, X., De Carlo, F.,
467 van Rossum, D. B., La Riviere, P., and K. C. Cheng, 2019. Computational 3D histological
468 phenotyping of whole zebrafish by X-ray histotomography. *eLife*. 8:e44898. doi:
469 10.7554/eLife.44898
470 10. Dion, V., 2014**.** Tissue specificity in DNA repair: lessons from trinucleotide repeat
471 instability. *Trends Genet*. 30(6): 220-9
472 11. Drenkard, E., Richter, B. G., Rozen, S., Stutius, L. M., Angell, N. A., Mindrinos, M., Cho,
473 R. J., Oefner, P. J., Davis, R. W., and F. M. Ausubel, 2000. A simple procedure for the
474 analysis of single nucleotide polymorphisms facilitates map-based cloning in *Arabidopsis*.
475 *Plant Physiol*. Dec; 124(4): 1483-92. doi: 10.1104/pp.124.4.1483.
476 12. Encalada, S. E., P. R. Martin, J. B. Phillips, R. Lyczak, D. R. Hamill *et al*, 2000. DNA
477 replication defects delay cell division and disrupt cell polarity in *Caenorhabditis elegans*
478 embryos. *Dev. Biol*. 15: 225-238
479 13. Foiani, M., F. Marini, D. Gamba, G. Lucchini, and P. Plevani, 1994. The B subunit of the
480 DNA polymerase alpha-primase complex in *Saccharomyces cerevisiae* executes an
481 essential function at the initial stage of DNA replication. *Mol. Cell Biol*. 13: 923-933
482 14. Foiani, M., G. Liberi, G. Lucchini, and P. Plevani, 1995. Cell cycle-dependent
483 phosphorylation and dephosphorylation of the yeast DNA polymerase alpha-primase B
484 subunit. *Mol. Cell Biol*. 15: 883-891
485 15. Ferrari, M., G. Lucchini, P. Plevani, and M. Foiani, 1996. Phosphorylation of the DNA
486 polymerase alpha-primase B subunit is dependent on its association with the p180
487 polypeptide. *J. Biol. Chem*. 271: 8661-8666

488 16. Gillooly, J. F., Hein, A., and R. Damiani, 2015. Nuclear DNA content varies with cell size
489 across human cell types. *Cold Spring Harb Perspect Biol*. **7** (7): a019091.
490 17. Grossi, S., Puglisi, A., Dmitriev, P.V., Lopes, M., Shore, D. 2004. Pol12, the B subunit of
491 DNA polymerase α, functions in both telomere capping and length regulation. *Genes Dev*.
492 18(9):992-1006
493 18. He, J., Zhang, G., Almeida, A. D., Cayouette, M., Simons, B. D., and W. A. Harris, 2012.
494 How variable clones build an invariant retina. *Neuron*. Sep 6;75(5):786-98
495 19. Hu, M. and S. S. Easter, 1999. Retinal neurogenesis: the formation of the initial central
496 patch of postmitotic cells. *Dev Biol*. Mar 15;207(2):309-21.
497 20. Hübscher, U., Maga, G., and Spadari, S. 2002. Eukaryotic DNA polymerases. *Annu. Rev.*
498 *Biochem*. 71:133-63
499 21. Iyama T. and D. M. Wilson 3rd, 2013. DNA repair mechanisms in dividing and non-
500 dividing cells. *DNA Repair (Amst)*. Aug; 12(8):620-36. doi: 10.1016/j.dnarep.2013.04.015.
501 Epub 2013 May 16.
502 22. Jevtić, P., Edens, L. J., Vuković, L. D., and D. L. Levy, 2014. Sizing and shaping the
503 nucleus: mechanisms and significance. *Curr Opin Cell Biol*. 28: 16-27.
504
23. Johnson, R. E., Prakash, L., and S. Prakash, 2012. Pol31 and Pol32 subunits of yeast DNA
505 polymerase δ are also essential subunits of DNA polymerase ζ. *Proc Natl Acad Sci U S A*.
506 109(31): 12455–12460.
507 24. Kaguni, L.S. and Lehman, I.R. 1988. Eukaryotic DNA polymerase-primase: structure,
508 mechanism, and function. *Biochim Biophys Acta*. 950:87-101
509 25. Kane, D.A. and C. B. Kimmel, 1993. The zebrafish midblastula transition. *Development*.
510 119:447-56.

511 26. Kim, E. K., Yoon, G., and H. S. Kim, 2016. Chemotherapy-induced endometrial pathology:
512 mimicry of malignancy and viral endometritis. *Am J Transl Res*. 8(5): 2459-2467
513 27. Klinge, S., Núñez-Ramírez, R., Llorca, O., and L. Pellegrini, 2009. 3D architecture of DNA
514 Pol α reveals the functional core of multi-subunit replicative polymerases. *EMBO J*. **28**:
515 1978-1987.
516 28. Kodota, K., Nitadori, J., Woo, K. M., Sima, C. S., Finley, D. J., Rusch, V. W., Adusumilli,
517 P. S., and W. D. Travis, 2014. Comprehensive pathological analyses in lung squamous cell
518 carcinoma: single cell invasion, nuclear diameter and tumor budding are independent
519 prognostic factors for worse outcomes. *J Thorac Oncol*. **9** (8): 1126-1139
520 29. Li, Z., Hu, M., Ochocinska, M. J., Joseph, N. M., and S. S. Easter Jr., 2000. Modulation of
521 cell proliferation in the embryonic retina of zebrafish (*Danio rerio*). *Dev*
522 *Dyn*. Nov;219(3):391-401.
523 30. Lynch, H. T. and A. de la Chapelle, 1999. Genetic susceptibility to non-polyposis
524 colorectal cancer. *J Med Genet*. 36 (11): 801-818.
525 31. Manimaran, D., Karthikeyan, T. M., Khan, D. M., and R. T. Raman, 2014. Follicular
526 variant of papillary thyroid carcinoma: cytological indicators of diagnostic value. *J Clin*
527 *Diagn Res*. **8** (3): 46-48
528 32. Mizuno, T., Yamagishi, K., Miyazawa, H., and F. Hanaoka, 1999 Molecular architecture
529 of the mouse DNA polymerase α-primase complex. *Mol Cell Biol*. 19(11):7886-96
530 33. Mohideen, M. P. K., Beckwith, L. G., Tsao-Wu, G. S., Moore, J. L., Wong, A. C. C.,
531 Chinoy, M. R., and K. C. Cheng, 2003 Histology-based screen for zebrafish mutants with
532 abnormal cell differentiation. *Developmental Dynamics*. 228:414-423

533 34. Nouspikel, T. and P. C. Hanawalt, 2000. Terminally differentiated human neurons repair
534 transcribed genes but display attenuated global DNA repair and modulation of repair gene
535 expression. *Mol Cell Biol*. Mar; 20(5): 1562-1570. doi: 10.1128/mcb.20.5.1562-1570.2000
536 35. Poropatich, K., Yang, J. C., Goyal, R., Parini, V., and X. J. Yang, 2016. Nuclear size
537 measurement for distinguishing urothelial carcinomas from reactive urothelium on tissue
538 sections. *Diagn Pathol*. 11(1): 57.
539 36. Rauwerda, H., Wackers, P., Pagano, J. F., de Jong, M., Ensink, W., Dekker, R., Nehrdich,
540 U., Spaink, H. P., Jonker, M., and T. M. Breit, 2016. Mother-Specific Signature in the
541 Maternal Transcriptome Composition of Mature, Unfertilized Zebrafish Eggs. *PLoS*
542 *One*. Jan 22;11(1):e0147151
543 37. Rosai, J., 2004. *Rosai and Ackerman's Surgical Pathology*. Maryland Heights: MO; Mosby,
544 an affiliate of Elsevier Inc.
545 38. Schier, A.F. 2007. The maternal-zygotic transition: death and birth of RNAs. *Science*.
546 316:406-7
547 39. Schub, O., Rohaly, G., Smith, R.W.P., Schneider, A., Dehde, S., Dornreiter, I., Nasheuer,
548 H.P. 2001. Multiple phosphorylation sites of DNA polymerase α-primase cooperate to
549 regulate the initiation of DNA replication *in vitro*. *J Biol Chem*. 276(41):38076-83.
550 40. Shen, J., Gilmore, E. C., Marshall, C. A., Haddadin, M., Reynolds, J. J., Eyaid, W., Bodell,
551 A., Barry, B., Gleason, D., Allen, K., Ganesh, V. S., Chang, B. S., Grix, A., Hill, R. S.,
552 Topcu, M., Caldecott, K. W., Barkovich, A. J., and C. A. Walsh, 2000. Mutations in PNKP
553 cause microcephaly, seizures and defects in DNA repair. *Nat Genet*. 42(3): 245-249

554 41. Shimoda, N., Knapik, E. W., Ziniti, J., Sim, C., Yamada, E., Kaplan, S., Jackson, D., de
555 Sauvage, F., Jacob, H., and M. C. Fishman, 1999. Zebrafish genetic map with 2000
556 microsatellite markers. *Genomics*. Jun 15;58(3): 219-32. doi: 10.1006/geno.1999.5824.
557 42. Stenbäck, F., 1978. Life history and histopathology of ultraviolet light-induced skin
558 tumors. *Natl Cancer Inst Monogr.* Dec; 50: 57-70.
559 43. Suwa, Y., Gu, J., Baranovskiy, A. G., Babayeva, N. D., Pavlov, Y. I., and T. H. Tahirov,
560 2015. Crystal structure of the human Pol α B subunit in complex with the C-terminal
561 domain of the catalytic subunit. *J Biol Chem*. 290(23): 14328-14337.
562 44. Tadros, W. and H. D. Lipshitz, 2009. The maternal-to- zygotic transition: a play in two
563 acts. *Development*. 136:3033-42
564 45. Uchiyama, M. and T. S. Wang, 2004 The B-subunit of DNA polymerase alpha-primase
565 associates with the origin recognition complex for initiation of DNA replication. *Mol. Cell*
566 *Biol*. 24: 7419-7434
567 46. Waga, S., Bauer, G., Stillman, B. 1994. Reconstitution of complete SV40 DNA replication
568 with purified replication factors. *J Biol Chem*. 269(14):10923-34
569 47. Wallace, K. N., Akhter, S., Smith, E. M., Lorent, K., and M. Pack, 2005. Intestinal growth
570 and differentiation in zebrafish. *Mech Dev*. Feb;122(2):157-73.
571 48. Wan, Y., Almeida, A. D., Rulands, S., Chalour, N., Muresan, L., Wu, Y., Simons, B. D.,
572 He, J., and W. A. Harris, 2016. The ciliary marginal zone of the zebrafish retina: clonal
573 and time-lapse analysis of a continuously growing tissue. *Development*. Apr
574 1;143(7):1099-107

575 49. Wang, Y. T., Tseng, T. L., Kuo, Y. C., Yu, J. K., Su, Y. H., Poss, K. D., and C. H. Chen,
576 2019. Genetic reprogramming of positional memory in a regenerating appendage. *Curr*
577 *Biol*. Dec 16;29(24):4193-4207.e4. doi: 10.1016/j.cub.2019.10.038. Epub 2019 Nov 27.
578 50. Yamaguchi, T., Kawahara, A., Hattori, S., Taira, T., Abe, H., Sanada, S., Akiba, J., Nishio,
579 S., Ushijima, K., Kamura, T., and M. Kage, 2015. Cytological nuclear atypia classification
580 can predict prognosis in patients with endometrial cancer. *Cytopathology*. 26 (3): 157-66.
581 51. Yang, H., D. Xiang, S. P. Venglat, Y. Cao, E. Wang *et al*, 2009 *PolA2* is required for
582 embryo development in *Arabidopsis*. *Botany.* 87: 626-634
583 52. Zhang, L., Kendrick, C., Jülich, D. and S. A. Holley, 2008. Cell cycle progression is
584 required for zebrafish somite morphogenesis but not segmentation clock function.
585 *Development*. 135 (12): 2065-2070.
586 53. Kuo, L. J. and L. X. Yang, 2008. Gamma-H2AX – a novel biomarker for DNA double-
587 strand beaks. *In Vivo*. 22 (3): 305-9.
588

589 **Acknowledgements**

590 **General**: We thank Margaret Hubley, Gail Broda, and Kathryn Early for help in maintaining wild-
591 type and mutant zebrafish lines and generating embryos; Jean Copper and Lynn Budgeon for help
592 in development of zebrafish histology. **Funding:** This work was supported by NIH: 5R01
593 AR052535 (PI: KCC) and the Jake Gittlen Laboratories for Cancer Research. **Author**
594 **contributions**: The project was conceived by KCC; research design was by AYL and KCC;
595 experiments were done by AYL and GKT; analysis was by AYL, GKT, and KCC; AYL and KCC
596 wrote the paper; KCA, DBVR, and VAC contributed to experimental design and editing.
597 **Competing interest**: The authors declare no conflict of interest.

Figures

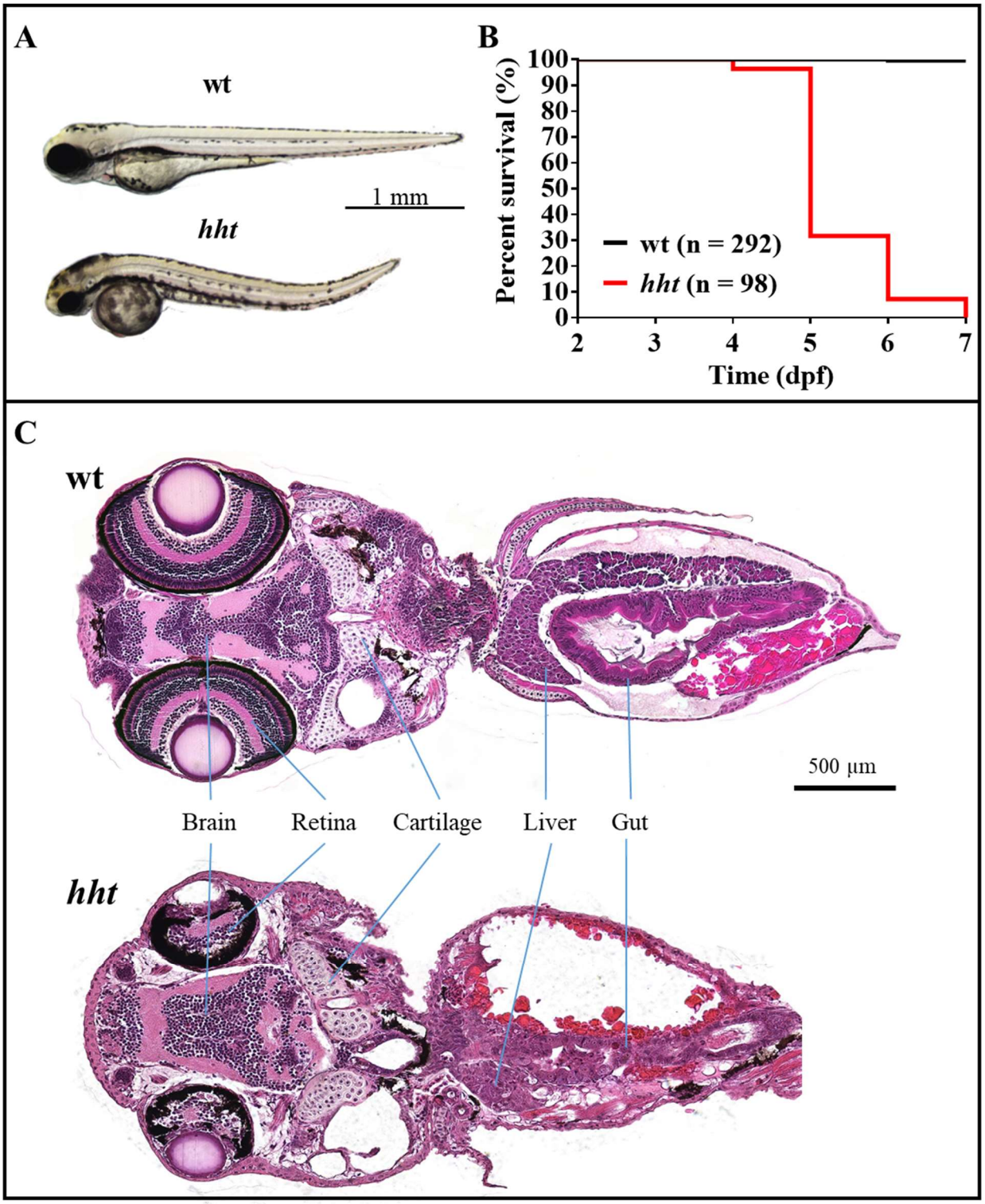
A
wt
1 mm
hht
B
Percent survival (%)
100
90
80
70
60
50
40
30
20
10
0
wt (n = 292)
hht (n = 98)
2
3
4
5
6
7
Time (dpf)
C
wt
500 µm
Brain
Retina
Cartilage
Liver
Gut
hht

Figure 1. The pleiotropic *hht* mutant survives up to 7 days. A) The *hht* mutant gross phenotype includes reduced head and eye size, an enlarged yolk, and dorsal curvature of the tail. **B)** The *hht* mutants show increasing larval lethality over 7 days; none survive past 7 days. In the same time period, only 1 wild-type sibling died. **C)** 5 dpf *hht* mutants exhibit disruption in tissue organization and a range of cellular dysmorphologies across most cell types.

600

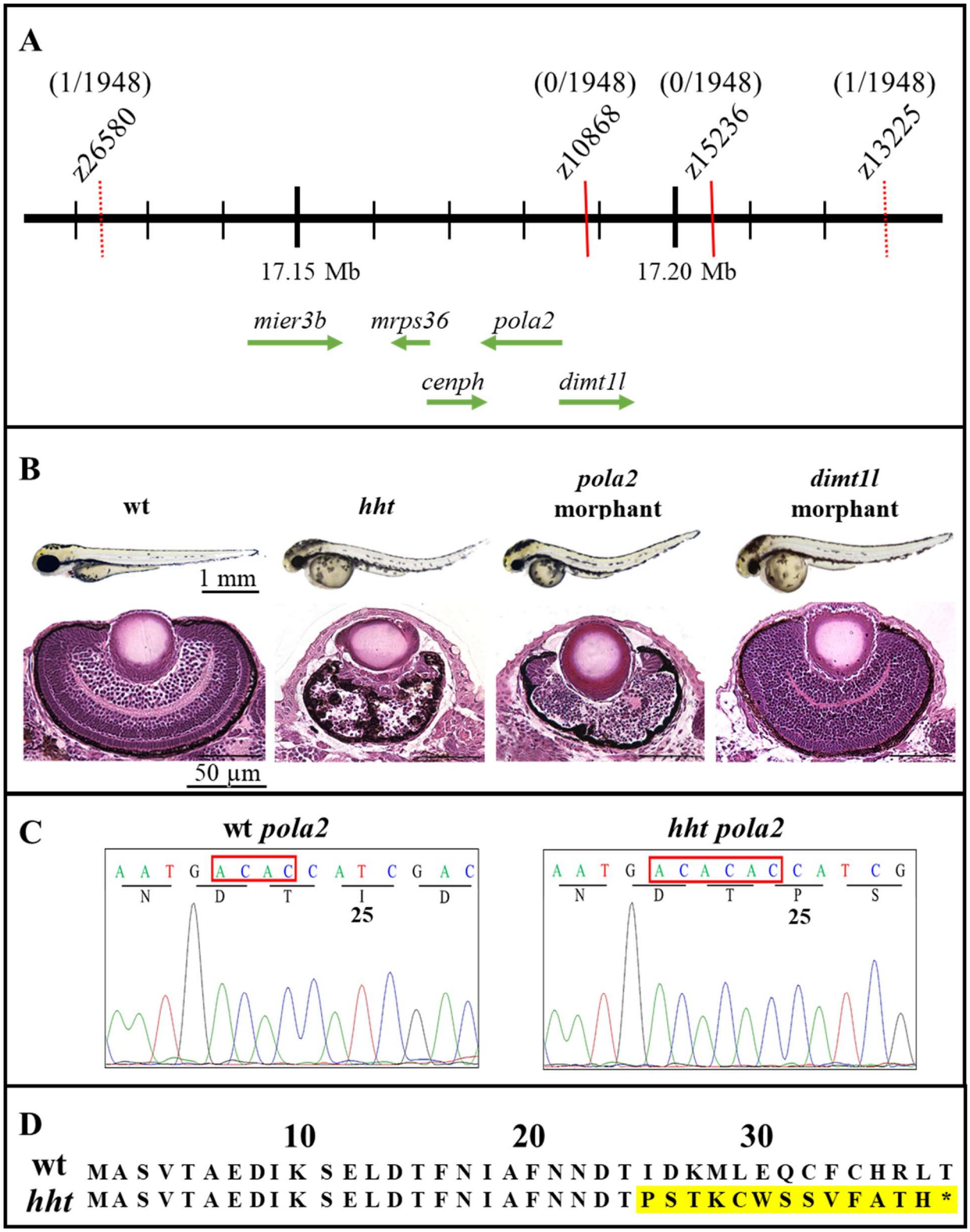
A
(1/1948)
(0/1948)
(0/1948)
(1/1948)
z26580
z10868
z15236
z13225
17.15 Mb
17.20 Mb
mier3b
mrps36
pola2
cenph
dimt1l
B
wt
hht
pola2 morphant
dimt1l morphant
1 mm
50 µm
C
wt pola2
hht pola2
A A T G A C A C C A T C G A C
N D T I D
25
A A T G A C A C A C C A T C G
N D T P S
25
D
10
20
30
wt M A S V T A E D I K S E L D T F N I A F N N D T I D K M L E Q C F C H R L T
hht M A S V T A E D I K S E L D T F N I A F N N D T P S T K C W S S V F A T H *

601

Figure 2. Microsatellite-based positional cloning of *pola2*. A) In positional cloning, the frequency of co-segregation of a phenotype of interest and polymorphic markers is used to locate the causative mutation. The map distance between the causative mutation and the markers is calculated from the frequency of recombinants as indicated above each marker. For markers *z26580* and *z13225*, 1 recombinant out of 1948 meiosis corresponds to ~ 0.05 centimorgans (cM), or 32.5 kb, in zebrafish. The lack of recombinants for markers *z10868* and *z15236* indicates that the causative mutation is physically closer to these two markers and resides in the interval between *z26580* and *z13225*. Five candidate genes, *mier3b* (mesoderm induction early response factor 1, family 3 b), *mrps36* (28S mitochondrial ribosomal protein S36), *cenph* (centromere protein H), *pola2* (DNA polymerase alpha, subunit B), and *dimtl1* (dimethyladenosine transferase), were annotated in the zebrafish genomic database in the identified GRCz11 region. **B)** Gross and histological examination of the eyes of wild-type, *hht*, *pola2* morphant, and *dimt1l* morphant revealed a striking similarity in reduced cell number, loss of stratification, thickened corneal epithelium, and disruption in the pattern of retinal pigmented epithelial pigment between *hht* and *pola2* morphant, suggesting that *pola2* was the affected gene in *hht*. **C)** a 2-nucleotitde AC insertion in the double AC repeat starting at the 68th nucleotide was detected in *hht.* **D)** This frameshift mutation results in changes in amino acid sequence starting at the 25th amino acid, ending with a premature stop codon at the 38th amino acid position. (red box = AC insertion; yellow highlight = amino acid change; asterisk = stop codon).

602
603

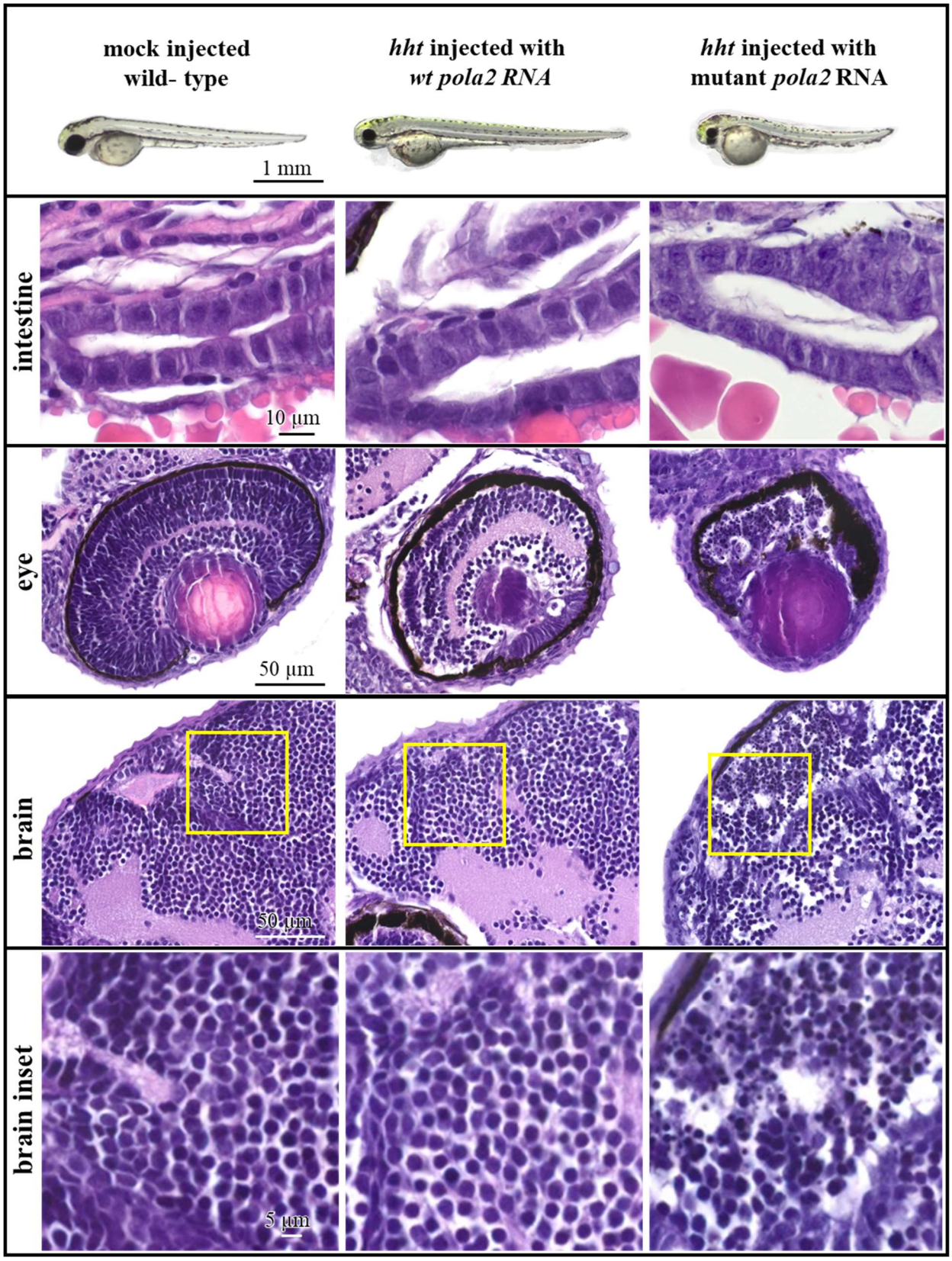
mock injected
wild- type
hht injected with
wt pola2 RNA
hht injected with
mutant pola2 RNA
1 mm
intestine
10 µm
eye
50 µm
brain
50 µm
brain inset
5 µm

604

Figure 3. Wild-type mRNA partially rescues the *hht* phenotype. Rescued *hht* mutants exhibit a straight body and a normal yolk. Sizes of the eyes and head are intermediate between wild-type and *hht* mutants. Rescued *hht* fish show histologically normal intestinal epithelium and partial preservation of the retinal layering found in wild-type eyes. The eyes and brain of partially rescued *hht* fish injected with wt mRNA show no evidence of nuclear fragmentation.

605
606

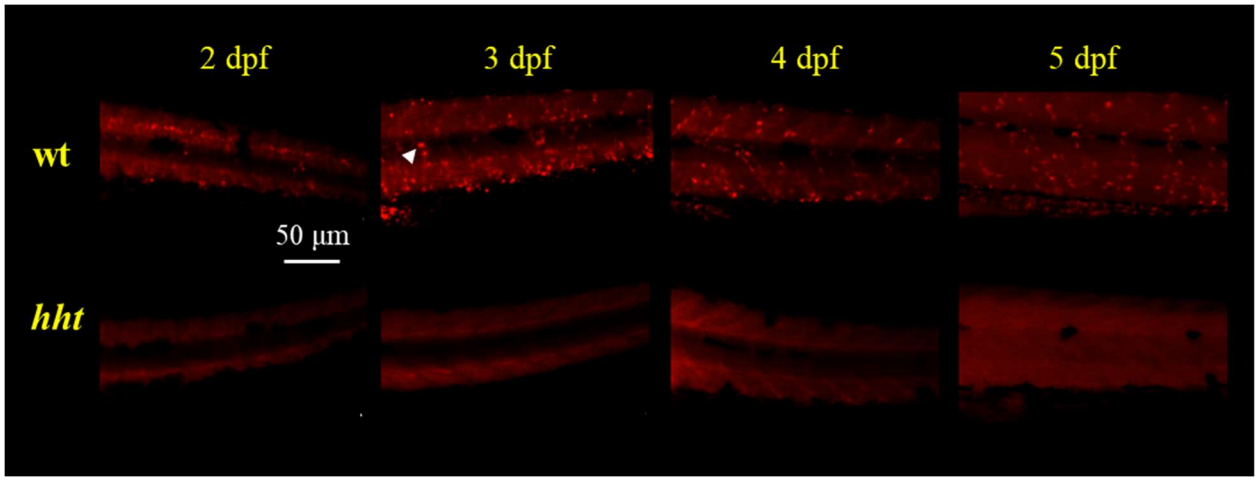

607
608

Figure 4. DNA synthesis is reduced in *hht* larvae. Representative images of wild-type and *hht* larvae stained with EdU. EdU-positive staining was observed in wild-type larvae, but absent in *hht* larvae at 48, 72, 96, and 120 hpf. 3 larvae were examined for each condition. White arrow = a positive focus.

609
610

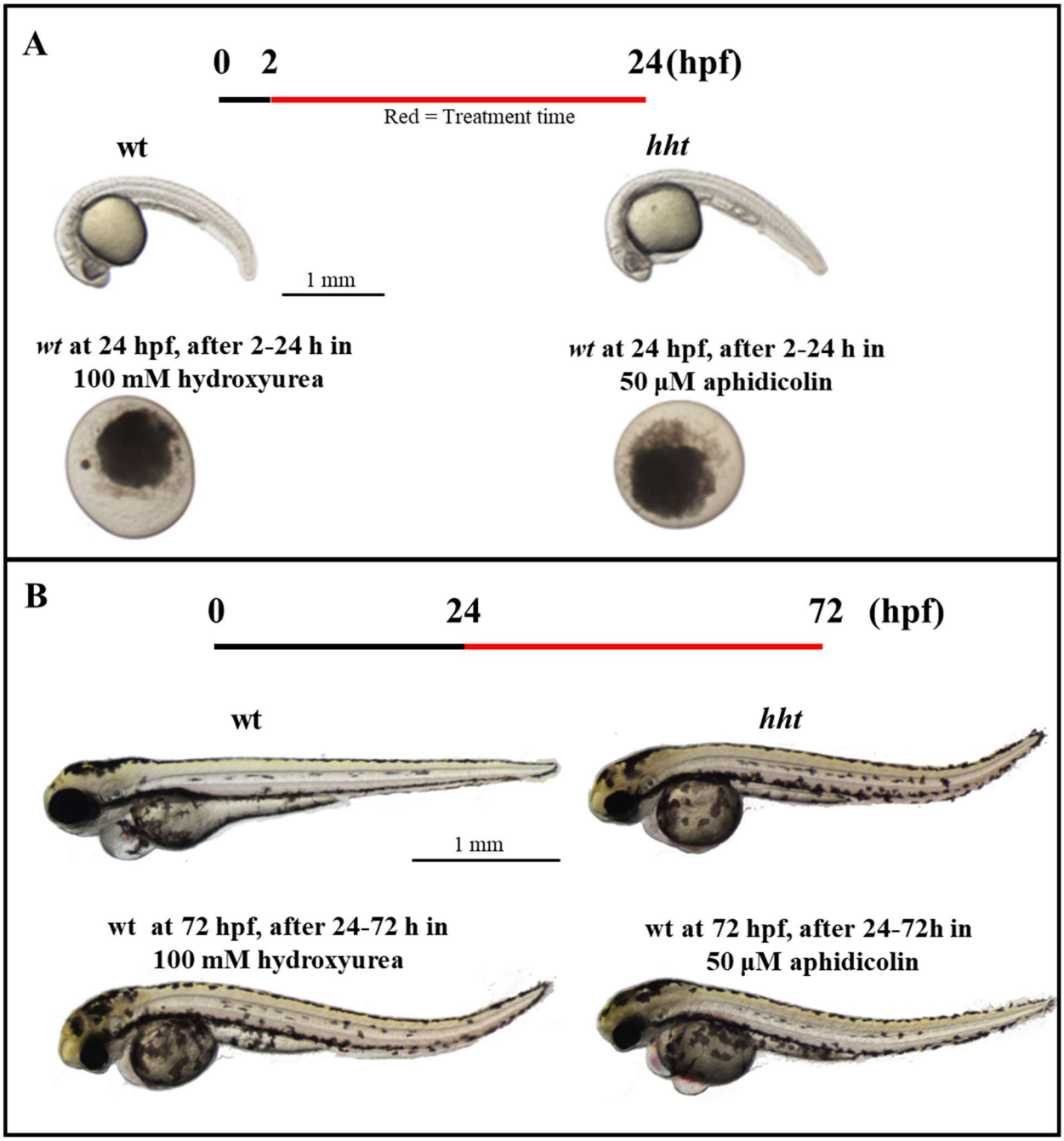

611

Figure 5. Chemical inhibition of DNA synthesis in *wt* larvae after 24 hours phenocopies *hht*. A) Treatment wild-type embryos with 100 mM hydroxyurea or 50 µM aphidicolin from 2 hpf on caused death by 24 hpf. **B)** Treatment of wild-type larvae (the time maternal wt *pola2* mRNA becomes undetectable) with 100 mM hydroxyurea or 50 µM starting at 24 hpf yields *hht* phenocopies at 72 hpf.

612

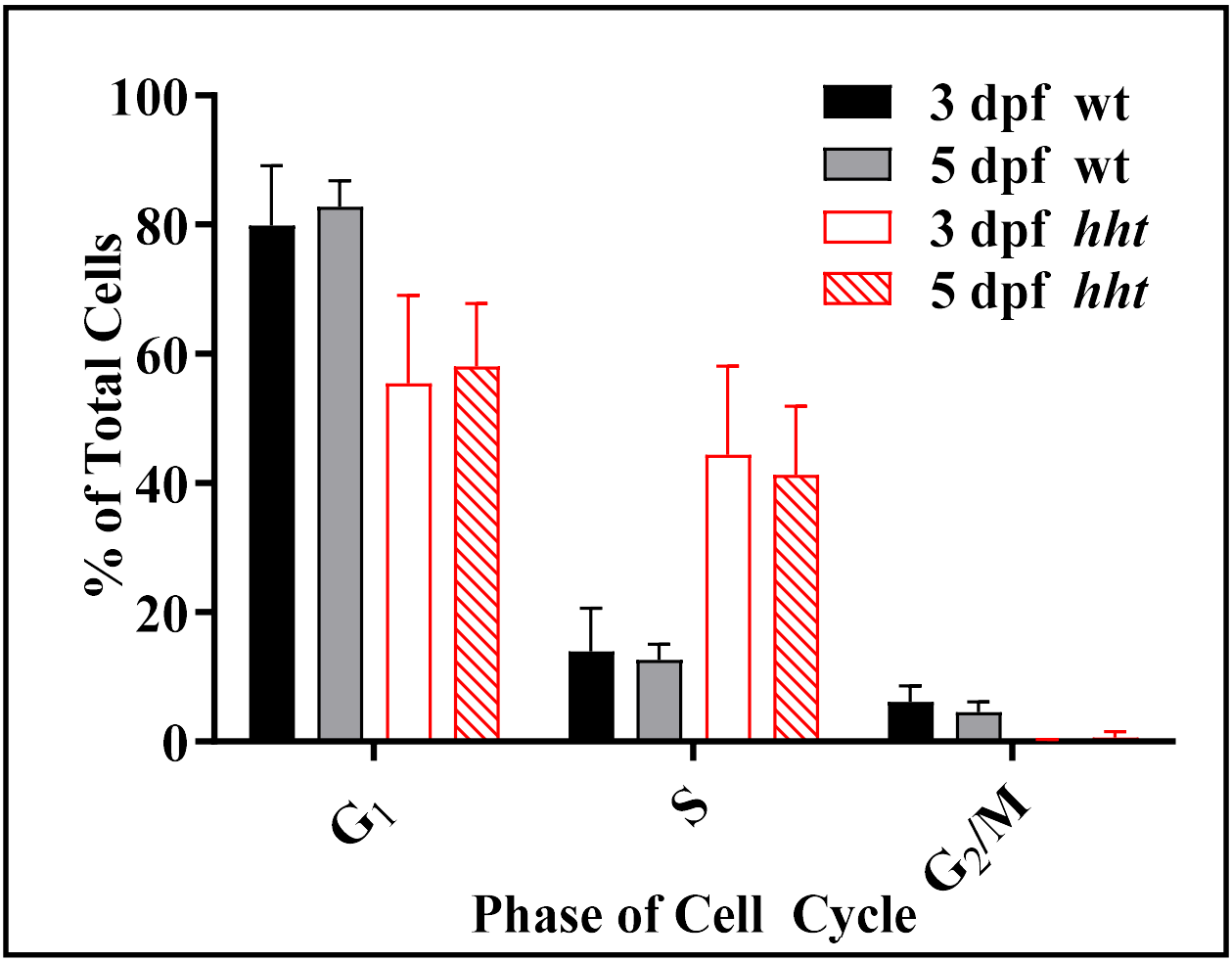

613

Figure 6. Accumulation of cells in S phase in *hht*. Wild-type and *hht* larvae were dissociated into single cells at 3 and 5 dpf, stained with propidium iodide, and analyzed by flow cytometry. Compared to wild-type, the proportion of cells in S phase increased significantly in *hht* at 3 dpf ($p < 0.05$) and persisted to 5 dpf ($p < 0.05$). Error bars = standard error of the mean.

614

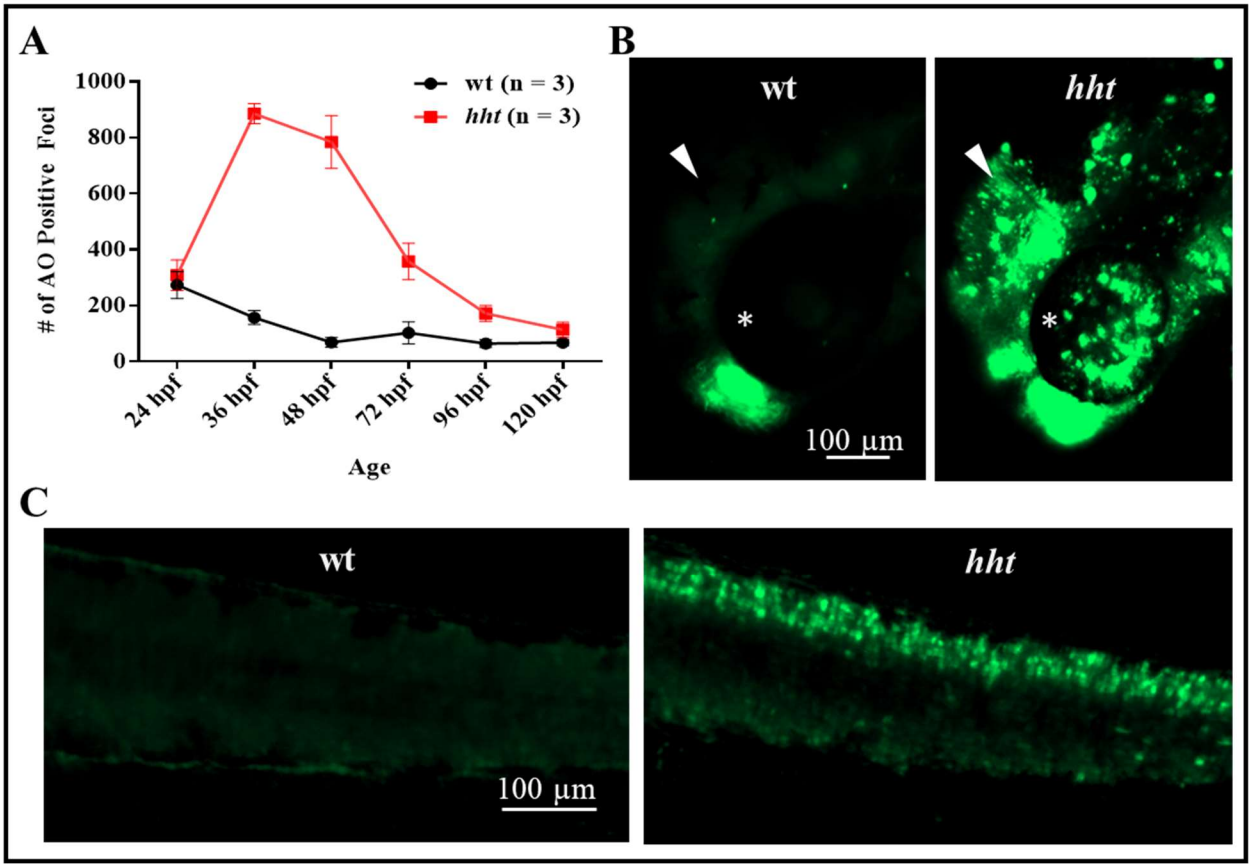

615
616

Figure 7. Acridine orange staining reveals increased cell death in the brain, eyes, and spinal cord of *hht* larvae. Cell death was assessed by counting the number of acridine orange-positive foci in 3 wild-type and 3 *hht* larvae. **A)** Cell death in *hht* was higher than in wild-type, peaking at 36 hpf. **B)** Cell death localized to the eyes and brain of 48 hpf *hht*. **C)** Cell death in the spinal cord in 48 hpf *hht*. Error bars = standard error of the mean. White arrow: brain, white asterisk: eye.

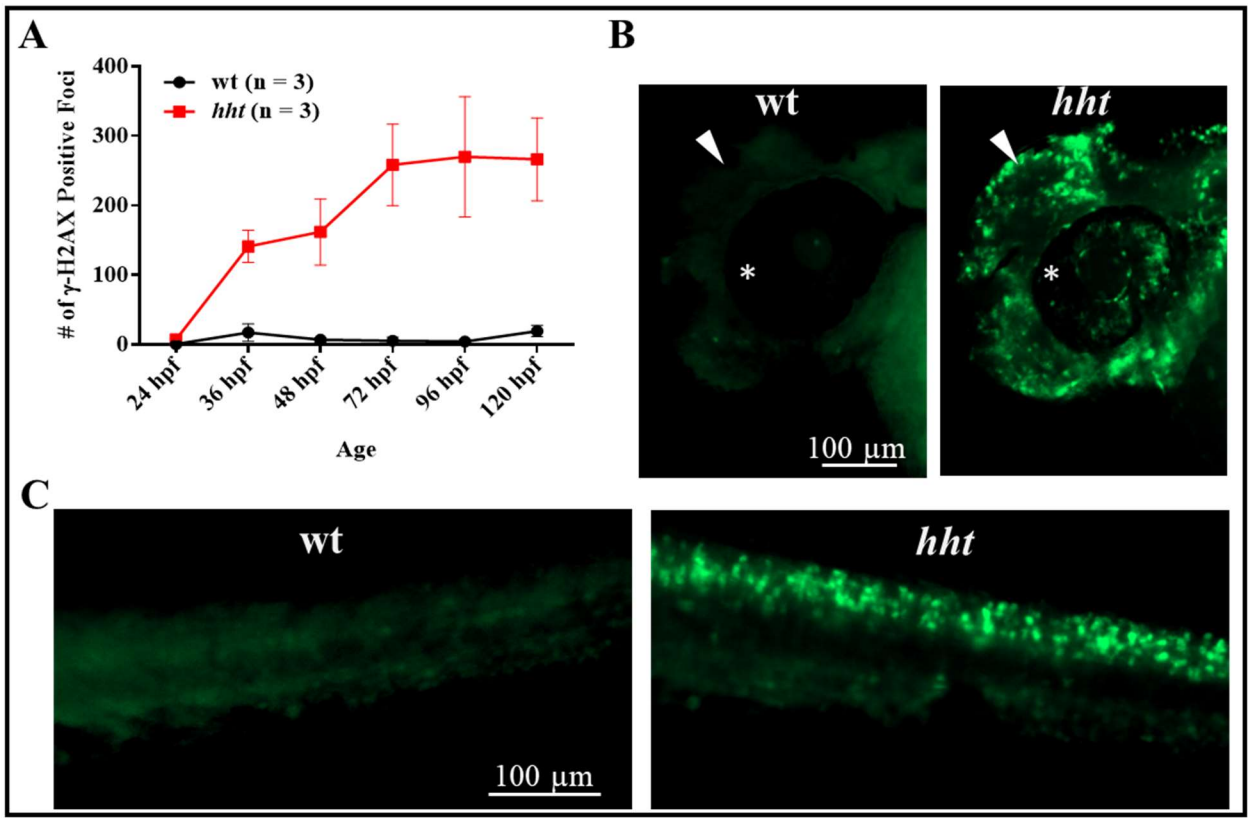

Figure 8. DNA damage is increased in *hht*. Double-stranded breaks were assessed by fluorescent antibody staining of γ-H2AX. **A)** DNA damage was minimal in wild-type, but striking in *hht* fish from 36-120 hpf. In 48 hpf *hht* fish, DNA damage was localized to the brain, eyes, and **B**) spinal cord **C**). Error bars = standard error of the mean. White arrow: brain, white asterisk: eye.

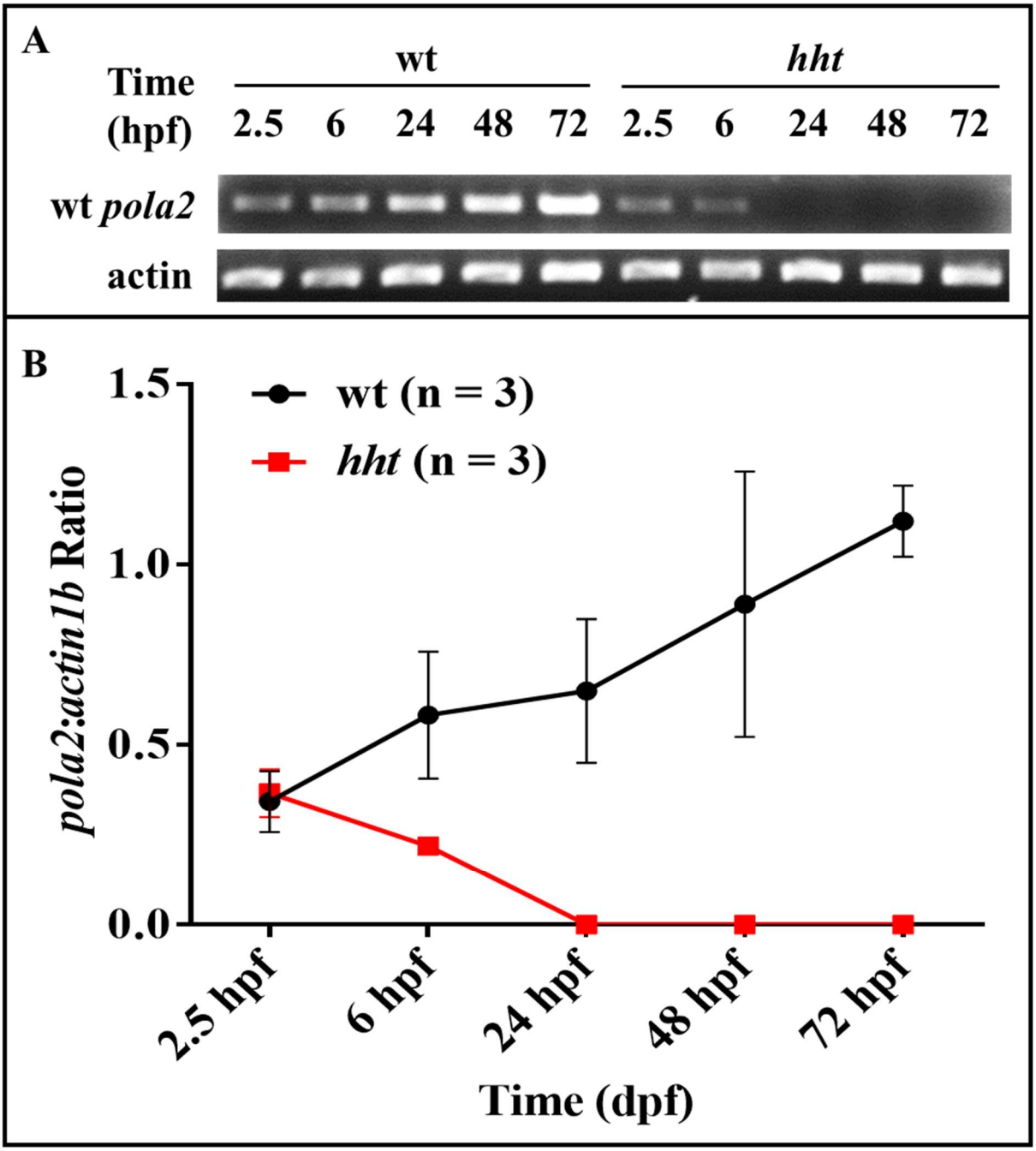

Figure 9. Wild-type *pola2* mRNA is detected in *hht* embryos. A) Wild-type *pola2* transcripts were detected in *hht* by allele-specific primers at 2.5 and 6 hpf. Wild-type transcripts were not detectable in *hht* after 24 hpf. **B)** Wild-type *pola2* transcripts were normalized to *actin1b*. Wild-type *pola2* transcripts in *hht* embryos were present at comparable levels to wild-type embryos at 2.5 hpf but were significantly reduced compared to wild-type embryos by 6 hpf ($p < 0.05$)

619

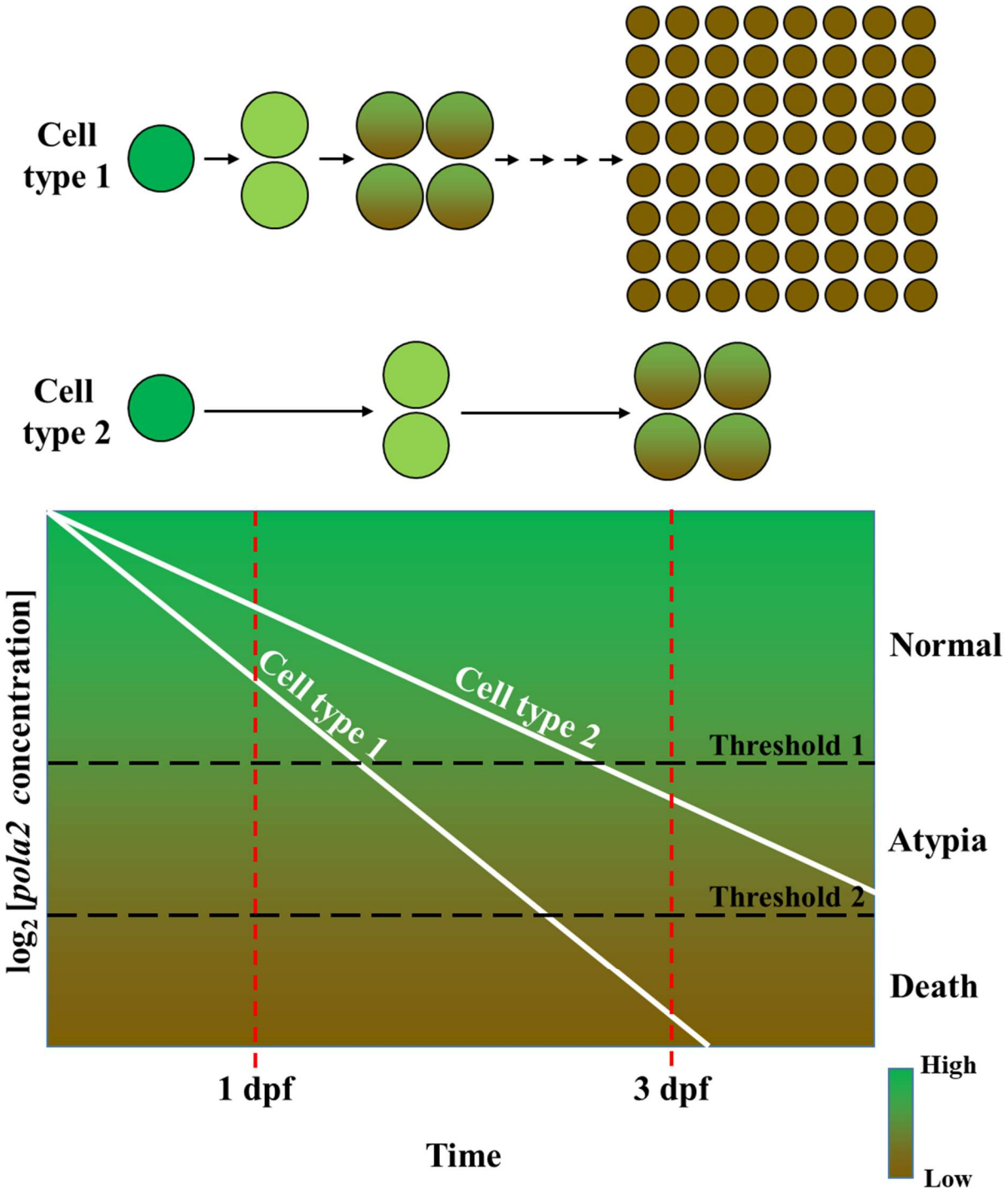
Cell type 1
Cell type 2
Normal
Atypia
Death
Threshold 1
Threshold 2
Cell type 1
Cell type 2
log2 [pola2 concentration]
1 dpf
3 dpf
Time
High
Low

620

Figure 10. Differential dilution of *pola2* accounts for tissue-specific differences in cell death. Homozygous *hht* mutant embryos cannot generate wild-type *pola2* mRNA. The quantity of wild-type *pola2* mRNA and protein, is diluted after each round of cell division. In this model, highly proliferative cell types undergo more cell divisions per unit time, resulting in lower concentrations of wild-type *pola2* mRNA or protein per cell compared to cell types that proliferate slowly. Nuclear atypia is apparent in cells with large nuclei but inapparent in cells with small, condensed nuclei.

621

622 **Tables**

623 ***Table 1: wild-type pola2 mRNA rescues hht mutants***

Injected mRNA	Total	$\frac{+}{+}$, $\frac{hht}{+}$	$\frac{hht}{hht}$	
		Phenotypically wild-type / (expected)	Partially rescued / total $\frac{hht}{hht}$	Phenotypically *hht*
None	182	136 / (137)	0 / 46	46
wt *pola2* RNA	302	234 / (227)	61 / 68	7
mutant *pola2* RNA	75	60 / (56)	0 / 15	15

624 A mixture of wild-type and mutant embryos from a $\frac{hht}{+}$ x $\frac{hht}{+}$ cross were injected at the 1-cell stage with phenol red, 200 pg wild-type *pola2* mRNA, or 200 pg mutant *pola2* mRNA. Number of embryos injected with no mRNA or wild-type *pola2* mRNA was aggregated from three separate experiments.

625

Supplementary Mateerials

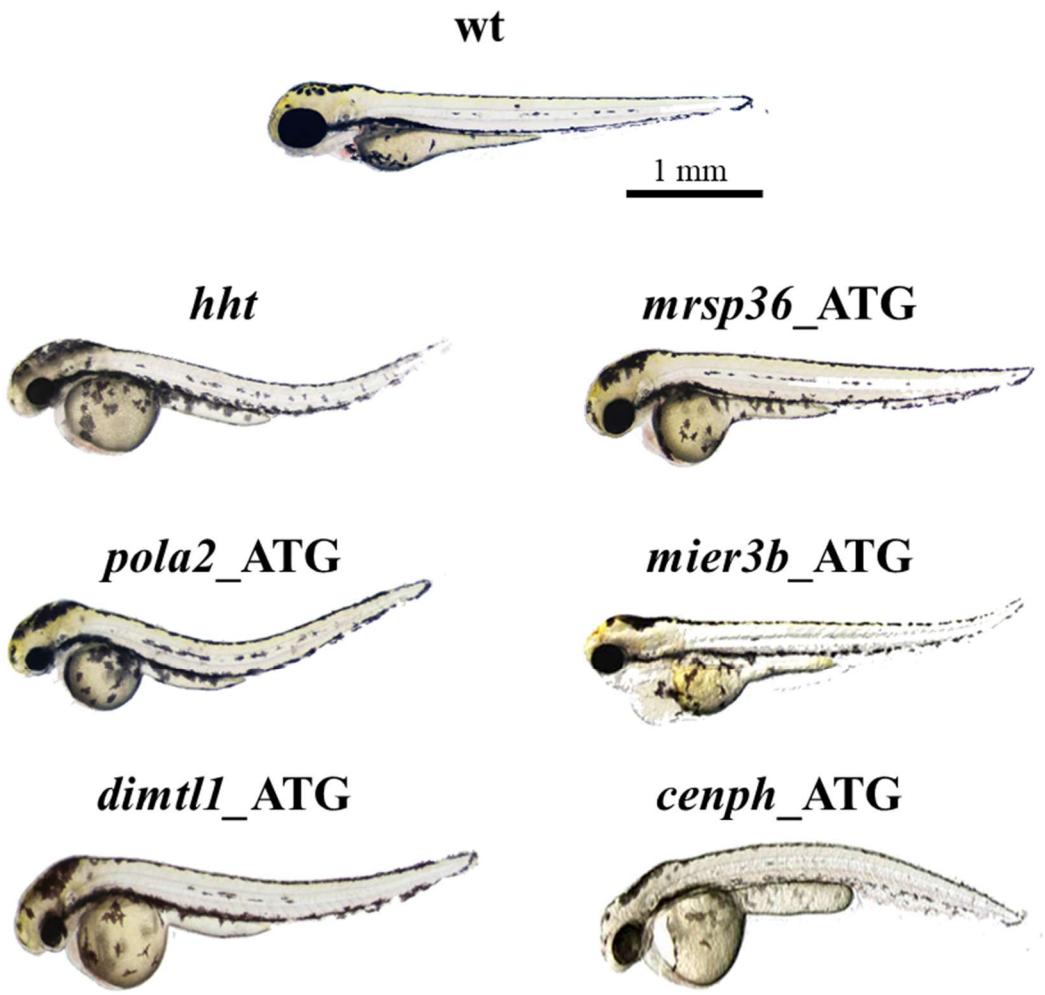

Supplemental S1. Morphants of the five candidate genes in the region identified by positional cloning, *mier3b*, *mrps36*, *cenph*, *pola2*, and *dimtl1*. Only *pola2* and *dimt1l* morphants exhibit a combination of small eyes, enlarged yolk, and dorsal curvature characteristic of *hht* mutants.

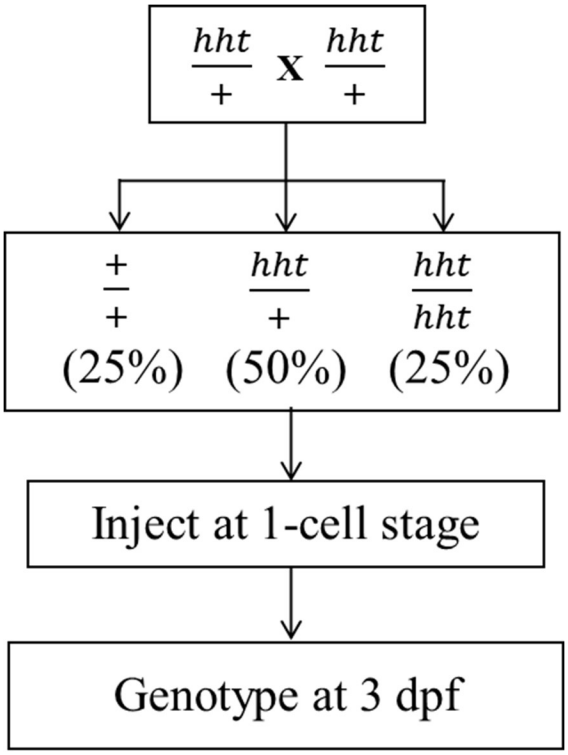

Supplemental S2. Wild-type *pola2* mRNA rescue schematic. Wild-type *pola2* mRNA was injected into 1-cell stage embryos from a $\frac{hht}{+}$ **X** $\frac{hht}{+}$ cross. Larvae were genotyped to confirm that rescued larvae were homozygous for the *hht* mutation.

A

```
wt   GTTGTTGTCATGGAAGGTATGAATCCCTC----------------GGGGGAGAAGCTTGTTGC
     |||||||||||||||||||||||||||#|#                |||||||||||||||||
hht  GTTGTTGTCATGGAAGGTATGAATCCATGACAACAGGGGGGAGAAGGGGGAGAAGCTTGTTGC
```

B

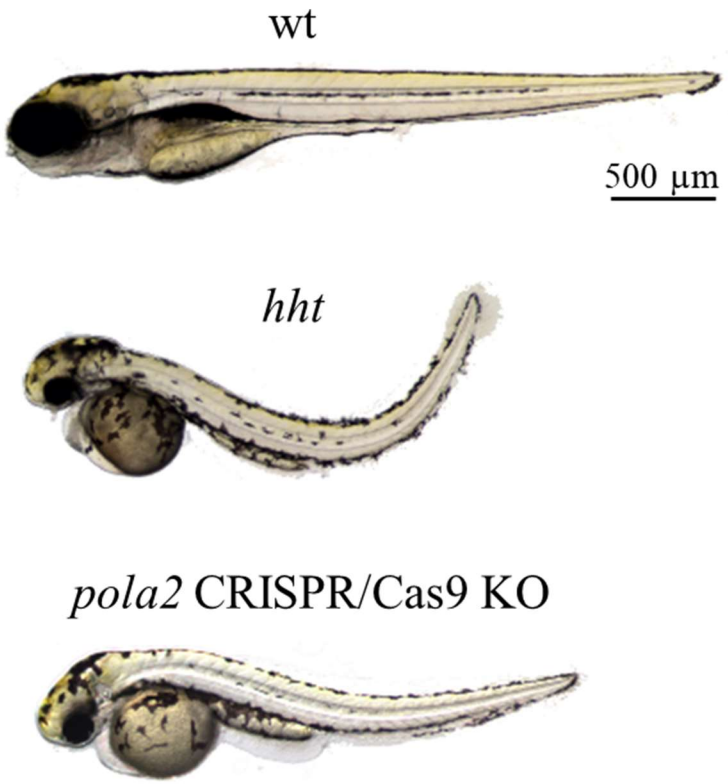

Supplemental S3. Shared phenotype of CRISPR/Cas9 *pola2* knockouts and *hht*

A) The CRISPR/Cas9 knockout zebrafish carried a 16-nucleotide insertion between nucleotides 927-928, causing a frameshift that changes the protein sequence after amino acid 308 in the 600-amino acid zebrafish Pola2 protein. Differences in severity in phenotype are consistent with variation in genetic background. **B**) Representative images of wild-type, *hht*, and *pola2* CRISPR/Cas9 knockout zebrafish larvae at 5 dpf. *hht* and *pola2* knockout fish shared small eyes, small head, enlarged and rounded yolk, and dorsally curved body.

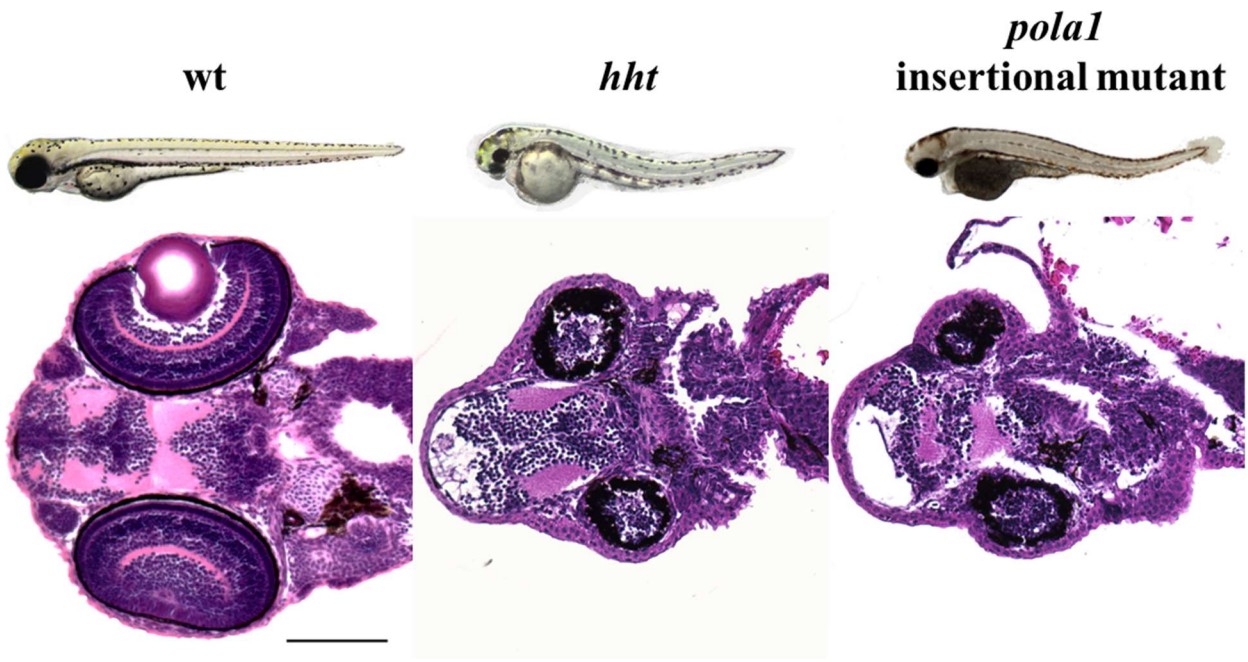

Supplemental S4. Mutants of *pola1* and *pola2* exhibit virtually indistinguishable gross and histological phenotypes. At 3 dpf, *hht*, our *pola2* null mutant, and a *pola2* insertional mutant both exhibit the combinatorial gross phenotype of small eyes, small head, rounded yolk, and curved body. Histologically, both mutants show a drastic reduction of cell number and loss of retinal layers in the eyes, reduced volume and disorganization of the white and gray matter of the brain. Scale bar = 100 μm.

Aphidicolin

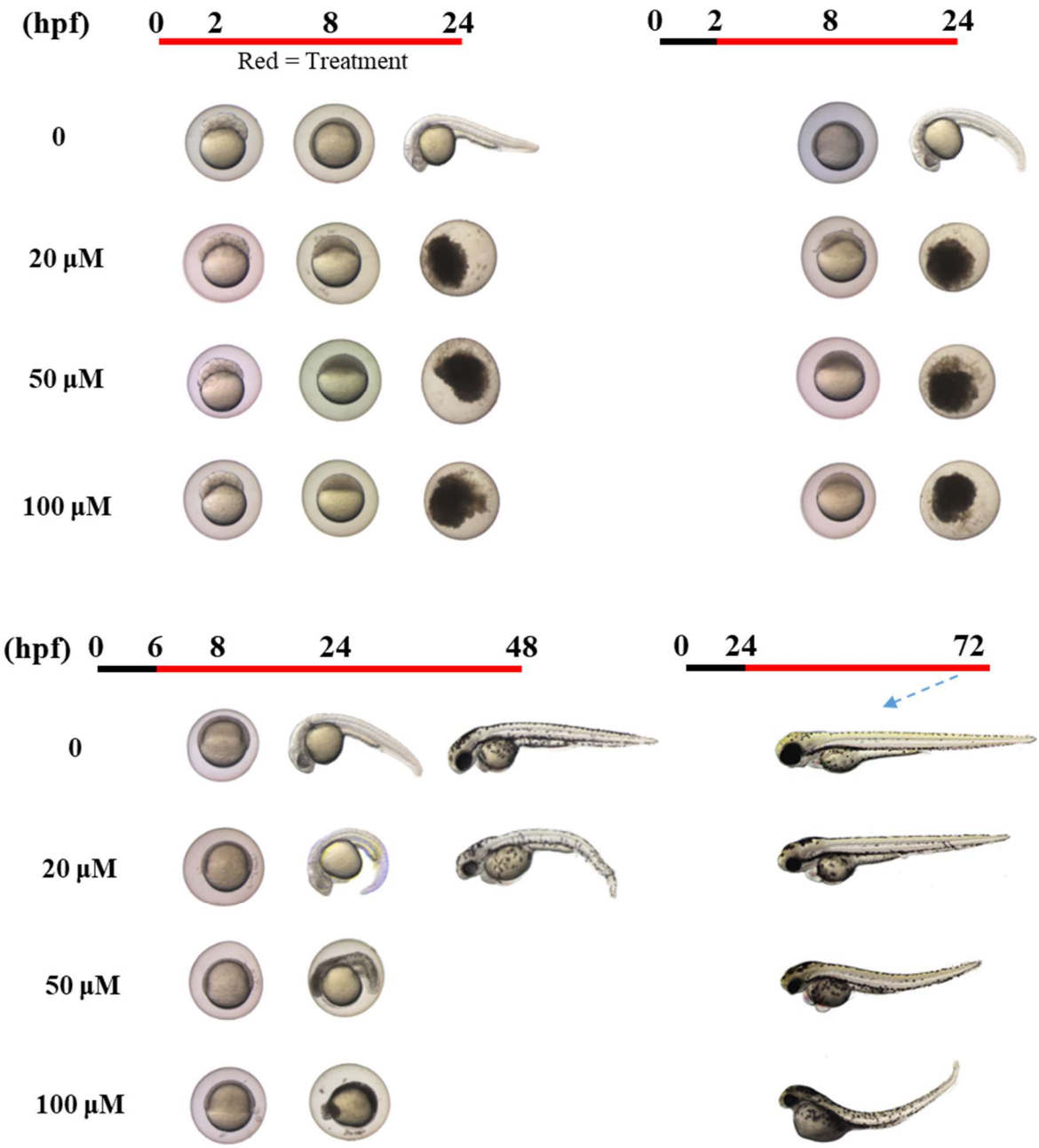

637

Supplemental S5. Inhibition of replicative DNA polymerases by aphidicolin beginning in wild-type zebrafish larvae at 24 hours, but not earlier, phenocopies *hht* at 72 hpf. Wild-type larvae were continuously exposed to 0, 20, 50, or 100 μM aphidicolin in DMSO. Treatment began at 0, 2, 6, or 24 hpf. 10 larvae were treated for each condition. Representative images are shown. Black line = no treatment; red line = treatment.

638

639

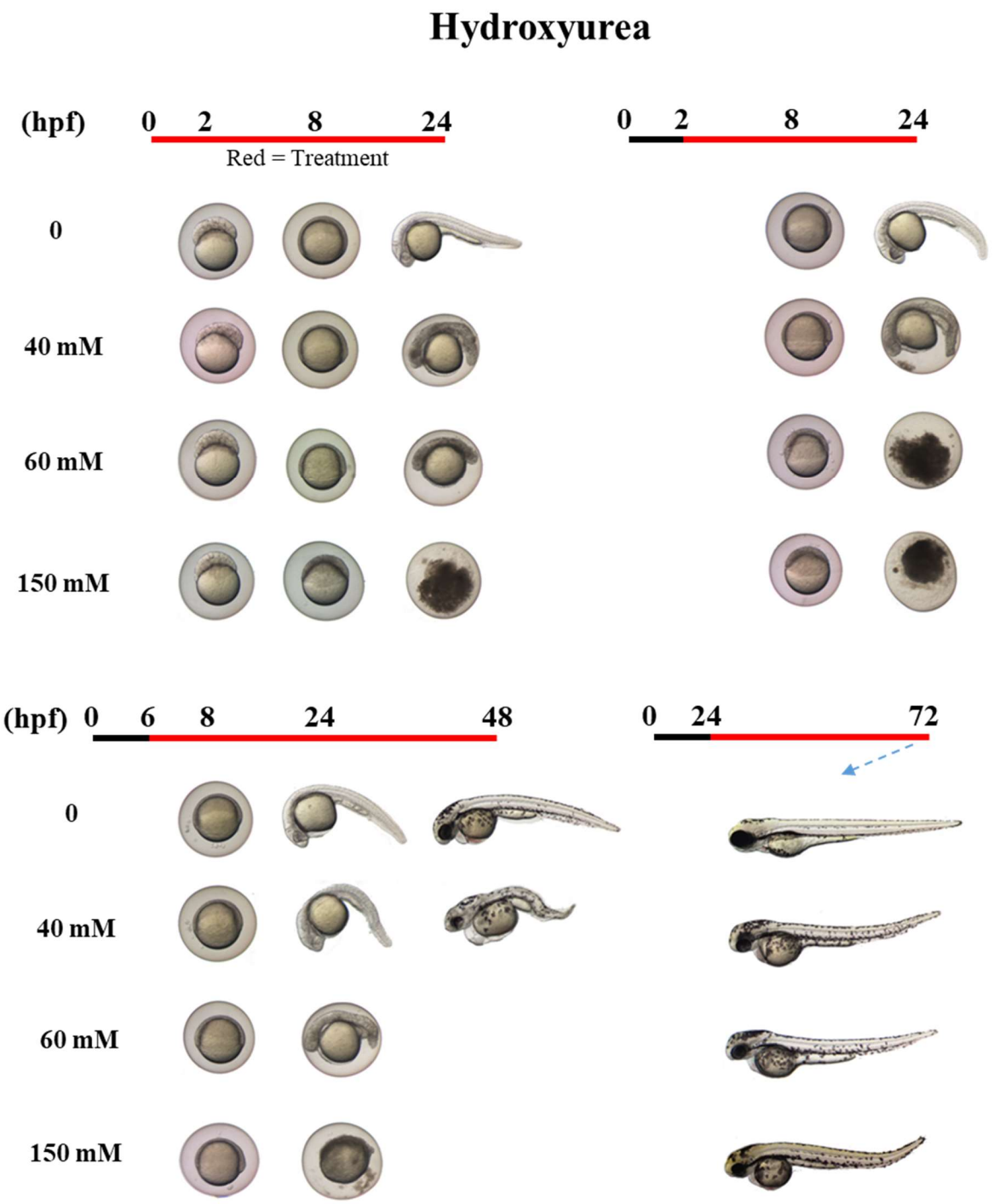
Hydroxyurea
(hpf)
0 2 8 24
Red = Treatment
0 2 8 24
0
40 mM
60 mM
150 mM
(hpf) 0 6 8 24 48
0 24 72
0
40 mM
60 mM
150 mM

640

Supplemental S6. Inhibition of deoxyribonucleotide production by hydroxyurea in wild-type zebrafish larvae beginning at 24 hours, but not earlier, phenocopies *hht* at 72 hpf. Wild-type larvae were continuously exposed to 0, 40, 60, or 150 mM aqueous hydroxyurea. Chemical treatment began at 0, 2, 6, or 24 hpf. 10 larvae were treated for each condition. Representative images are shown. Black line = no treatment; red line = treatment.

641

642

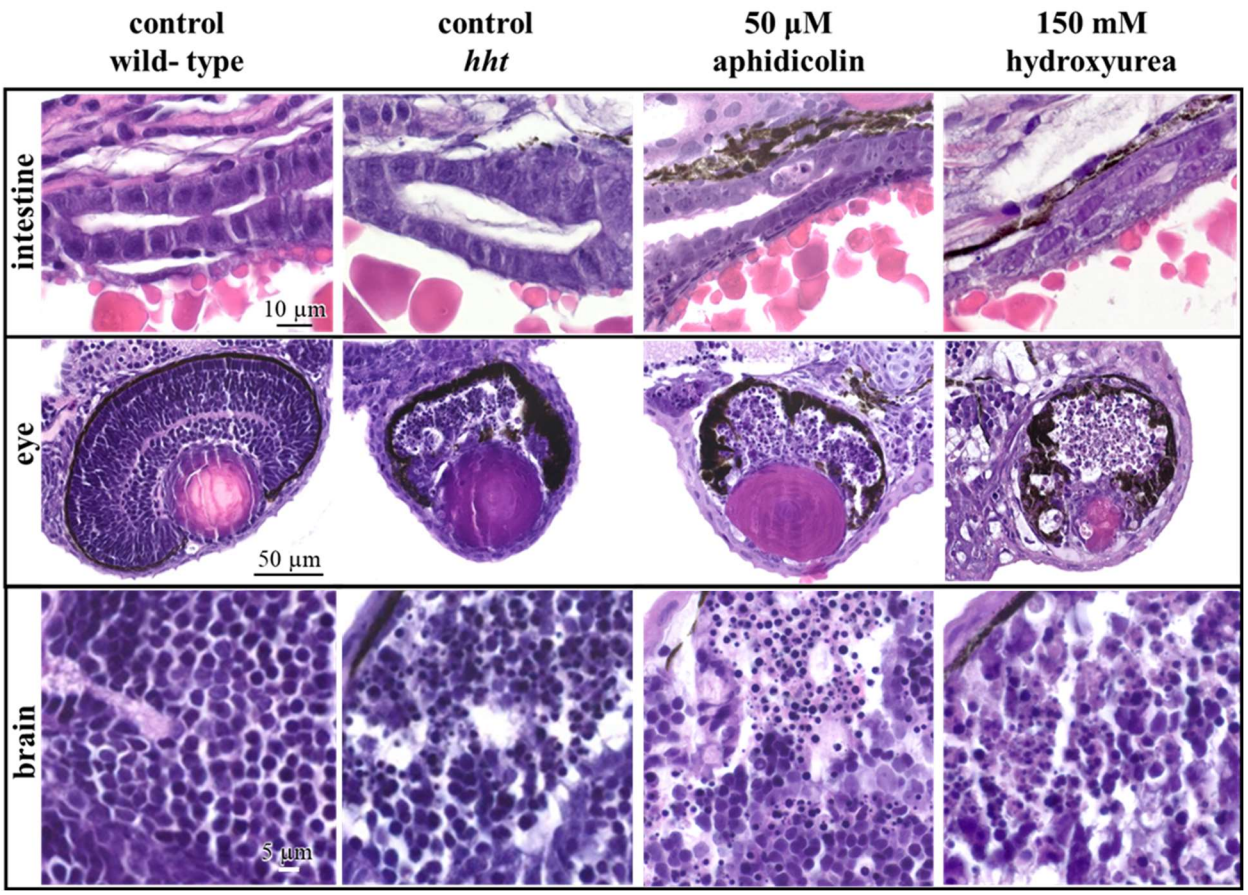

Supplemental S7. Chemical inhibition of DNA synthesis starting at 24 hpf phenocopies *hht* cellular phenotypes. Continuous exposure of wild-type larvae to 50 µm aphidicolin or 150 mM hydroxyurea starting at 24 hpf results in nuclear fragmentation in the prefrontal cortex and eyes. Eyes also suffer a drastic reduction in cell number and organization of retinal layers. Cellular and nuclear atypia are observed in the intestine – cell and nuclear sizes are irregular, cell boundaries are obscure, and prominent nucleoli are present.